Novel Hybrid Models by Coupling Support Vector Regression (SVR) With Meta-heuristic Algorithms (WOA and GWO) for Urban Flood Risk Mapping

Fatemeh Rezaie
KIGAM: Korea Institute of Geoscience and Mineral Resources
Mahdi Panahi
KIGAM: Korea Institute of Geoscience and Mineral Resources
Sayed M. Bateni
UH Manoa: University of Hawai'i at Manoa
Changhyun Jun
Chung-Ang University - Seoul Campus: Chung-Ang University
Christopher Neale
Nebraska Christian College
Saro Lee (leesaro@kigam.re.kr)
Korea Institute of Geoscience and Mineral Resources https://orcid.org/0000-0003-0409-8263

Research Article

Keywords: Flood risk map, Grey wolf optimizer, Whale optimization algorithm, SVR, Frequency ratio, Iran

Posted Date: March 17th, 2022

DOI: https://doi.org/10.21203/rs.3.rs-1133388/v1

Novel hybrid models by coupling support vector regression (SVR) with meta-heuristic algorithms (WOA and GWO) for urban flood risk mapping

Fatemeh Rezaie[1, 2], Mahdi Panahi[3], Sayed M. Bateni[4], Changhyun Jun[5*],

Christopher Neale[6], Saro Lee[1, 2 *]

[1] Geoscience Platform Research Division, Korea Institute of Geoscience and Mineral Resources (KIGAM), 124, Gwahak-ro, Yuseong-gu, Daejeon 34132, Republic of Korea; rezaie@kigam.re.kr

[2] Department of Geophysical Exploration, Korea University of Science and Technology, 217, Gajeong-ro, Yuseong-gu, Daejeon 34113, Republic of Korea; leesaro@kigam.re.kr

[3] Division of Smart Regional Innovation, Kangwon National University, 1 Gangwondaehak-gil, Chuncheon-si, Gangwon-do, 24341, Republic of Korea; mahdi.panahi@kangwon.ac.kr

[4] Department of Civil and Environmental Engineering and Water Resources Research Center, University of Hawaii at Manoa, Honolulu, Hawaii, USA, 96822; smbateni@hawaii.edu

[5] Department of Civil and Environmental Engineering, College of Engineering, Chung-Ang University, Seoul 06974, Korea; cjun@cau.ac.kr

[6] Daugherty Water for Food Global Institute, University of Nebraska, Lincoln, Nebraska, USA; cneale2@unl.edu

Abstract

Schools as social bases and children's centers are among the most vulnerable areas to flooding. Flood risk mapping (FRM) is very important for flood preparedness and adopting preventive plans for reducing the school vulnerability to flooding. To achieve this, there is a need for the models that can be used in vast areas with high predictive accuracy. This study aims to develop the innovative hybrid models by coupling the support vector regression (SVR), statistical approaches, and two meta-heuristic algorithms, whale optimization algorithms (WOA) as well as grey wolf optimizer (GWO). According to the proposed

methodology, a hybrid feature of SVR and frequency ratio (FR-SVR) is optimized by applying the GWO and WOA optimization algorithms to generate the maps related to flood susceptibility (FSMs). The method was utilized for the Ardabil Province located in southwestern Caspian Sea precincts of which faced devastating floods. The GIS database including 147 ground control locations of flooded zones and nine factors which influence flood were utilized to learn and ascertain the validity of the models. The statistical measures of RMSE, MAE, AUC, and ROC curve were then applied for the developed models in order to estimate prophetically. The results indicated that the meta-optimized FR-SVR-GWO as well as FR-SVR-WOA models exceeded the FR-SVR and FR models in training ($RMSE_{FR\text{-}SVR\text{-}WOA}$ = 0.2016, $RMSE_{FR\text{-}SVR\text{-}GWO}$ = 0.1885, $AUC_{FR\text{-}SVR\text{-}WOA}$ = 0.87, $AUC_{FR\text{-}SVR\text{-}GWO}$ = 0.88) and validation ($RMSE_{FR\text{-}SVR\text{-}WOA}$ = 0.2025, $RMSE_{FR\text{-}SVR\text{-}GWO}$ = 0.1986, $AUC_{FR\text{-}SVR\text{-}WOA}$ = 0.87, $AUC_{FR\text{-}SVR\text{-}GWO}$ = 0.87) phases. The FR-SVR-WOA and FR-SVR-GWO models were very competitive regarding AUC and RMSE values, but the FR-SVR-WOA model reproduced greater flood susceptibility rates and was considered for school flood risk mapping (SFRM).

Keywords: Flood risk map, Grey wolf optimizer, Whale optimization algorithm, SVR, Frequency ratio, Iran.

1. Introduction

Flood is a natural malware phenomenon that causes serious socio-economic damages worldwide. Based on "Global Assessment Report on Disaster Risk Reduction" (UNISDR, 2015), in North Africa as well as the Middle East countries is increasing yet due to the danger of mortality as a result of global flood although this danger has been decreased since 2000. Gholamian and Yousefian (2017) emphasized that in the year 2015 mortality rate of flood has increased up to 11% in the North Africa and Middle East countries in comparison with the previous century. The GDP percent exposed to floods has also tripled from the 1970s to

2000s in these countries (Centre for Research on the Epidemiology of Disasters, 201AD; UNISDR, 2015). Between 1981 and 2010 over eighty percent of events related to natural disaster in the MNA were accumulated in six states, including The Islamic Republic of Iran (UNISDR, 2015). Over several years ago, there have been several devastating natural disasters which the most important ones was flooding that occurred in Iran. Flood alone has killed one hundred and twelve people and has devastated 45000 domiciles during past two years. Many facilities for municipal services and farming lands as well as roads have been damaged.

Among the most vulnerable areas to flooding, schools are very important and should be paid special attention not only because of the children vulnerability during the flooding (Rufat et al., 2015), but also their exposure to post disaster problems. The young students are the worth affected people in flooding because of their physical, psychological, and social vulnerabilities. It is undeniable that we cannot prevent flood completely; however, flood proofing the existing schools in vulnerable areas and construction of new schools in areas with lower flood risk can dramatically minimize the damages.

Literature for detecting areas prone to flood shows that scholars have not only suggested but also implemented different data driven and statistical models. The only samples which suggest by scholars are analytical hierarchy process (AHP) (Ghosh and Kar, 2018; Seejata et al., 2018; Swain et al., 2020), frequency ratio (FR) (Rahmati et al., 2016; Waqas et al., 2021), evidential belief function (EBF) (Yariyan et al., 2020), weights-of-evidence (Khosravi et al., 2016a), and logistic regression (LR) (Shafapour Tehrany et al., 2017). Nevertheless, the aforementioned approaches are not free of shortcomings when devising the map for susceptibility to flood (FSM). For instance, the outcomes resulting from the AHP model are subjected to discrepancies due to the biased experts' verdict (Miles and

75 Snow, 1984). In addition, the results of the FR model largely hinge upon the size of sample
76 (McLay et al., 2001).

77 To overcome such problems, machine learning (ML) techniques (e.g., group method
78 of data handling (GMDH), artificial neural networks (ANNs), Naïve Bayes Trees (NBT),
79 support vector regression (SVR), and random forest (RF)) have been posed in the literature
80 (Band et al., 2020; Costache et al., 2021; Dodangeh et al., 2020; Khoirunisa et al., 2021;
81 Khosravi et al., 2018). However, machine learning techniques also suffer from strict
82 parameters tuning procedure which is time-consuming for modelers (Chen et al., 2019, 2017).
83 For the use of machine learning techniques, modelers have to either tune the model
84 parameters manually through the trial and error experiment (that is not cost effective) or
85 remain them as default which strictly affects the model performances (Leuenberger et al.,
86 2018). This is especially more important for modeling highly non-linear relationships, such as
87 flood modeling, which forces the modeler to take enduring attempts to achieve desired
88 results. The SVR model has been proven as a rigorous ML method which has been rarely
89 applied in hydrological applications. The SVR model suffers from difficulties due to the
90 optimization of the model and finding the best weights of the parameters that severely affects
91 the model's prediction capability (Wang and Xu, 2017). It is also slow in terms of speed for
92 training and is noise-sensitivity in hydrological modeling (Balogun et al., 2021; Panahi et al.,
93 2021; Siam et al., 2021). The downward approach of gradient is commonly used for tuning
94 the SVR parameters. In this approach, the gradient is calculated during several iterations and
95 each time its performance is influenced by the initial point (Ewees and Elaziz, 2018). The
96 meta-heuristic optimization algorithms can be considered as potential solutions to alleviate
97 the difficulties associated with the parameter-tuning the SVR model (Ewees and Elaziz,
98 2018; Jaafari et al., 2019). These algorithms allows a automatically parameter estimation of
99 the machine learning models (Razavi Termeh et al., 2018) and improve the model

100 performance. Imitating the biological phenomena, scientists have propounded various meta-
101 heuristic algorithms to manage the optimization problems (e.g., Mirjalili and Lewis, 2016).

102 In this study, two meta-heuristic algorithms, GWO (Mirjalili et al., 2014) and WOA
103 (Mirjalili and Lewis, 2016) were used to optimize the SVR structure. The new hybrid models
104 called FR-SVR-WOA and FR-SVR-GWO will be used to develop the flood susceptibly map
105 at northwest of Iran, Ardebil Province. Many studies almost stopped in this stage by
106 providing a map which demonstrates the flood vulnerability areas. Even, in this research, we
107 went a step further to generate Flood Risk Map (FRM) by taking into account school
108 vulnerability indices such as number of schools, area of the school buildings, and number of
109 students per each school. Figure 1 shows the graphical demonstration of the model
110 development and flood risk map preparation.

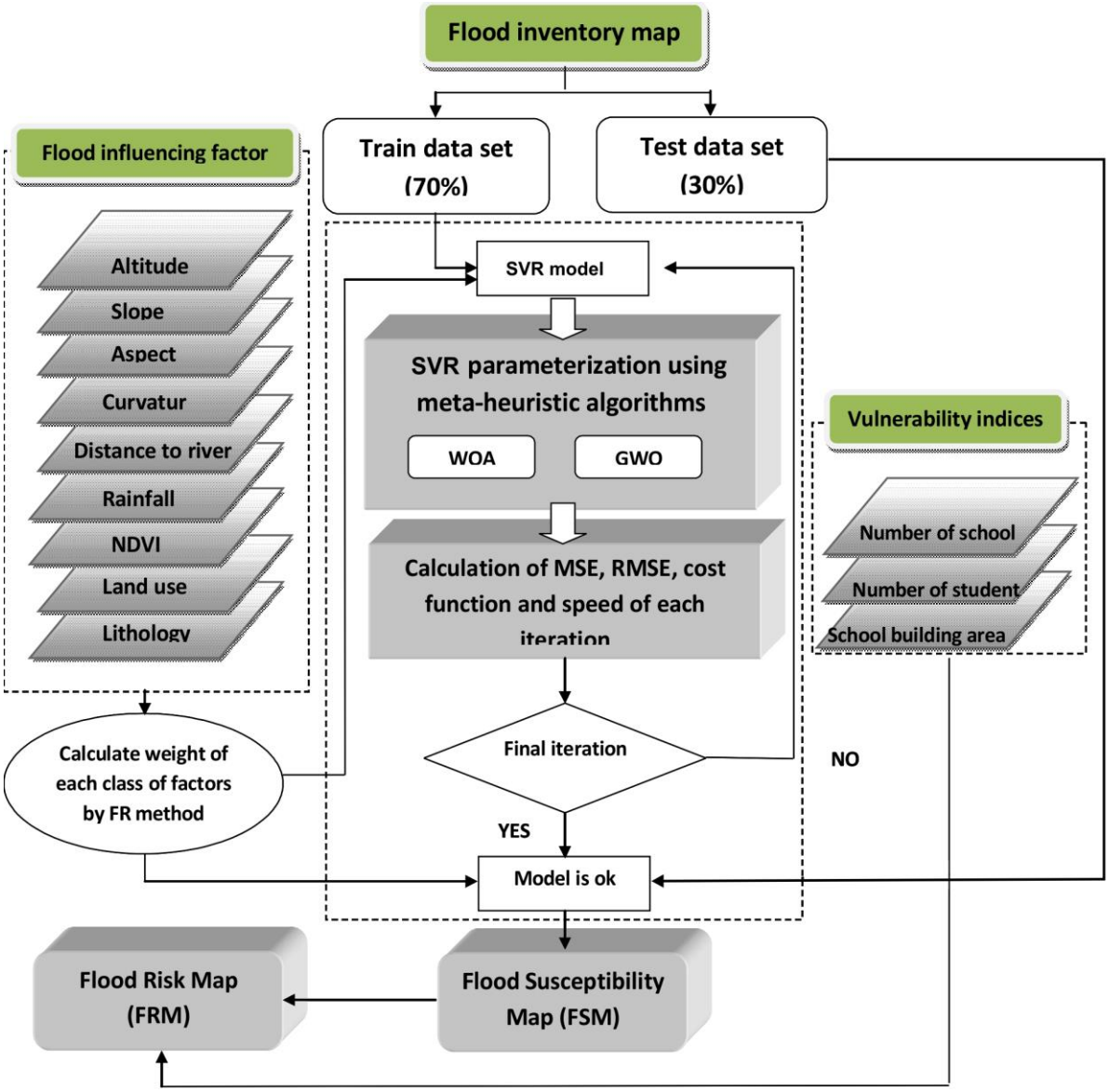

Figure 1. Flowchart of the research representing the model development for flood susceptibility modeling and risk mapping

2. Description of the area under study

The area under study encompasses the province of Ardabil in Iran's northwest. This province covers an area of around 17,953 km^2 which is one percent of the country's area and Talesh Mountains are at its east and being restricted on the west by Azerbaijan Plateau (Tavoosi and Delara, 2010) (Figure 2). About three-quarter of land area in this province consists of mountains and hills, reaching the highest elevation of 4811 meters at Sabalan Mountain. Due to complex topography and presence of several lakes, this region has a very varied climates from semi-humid and Mediterranean climate in the south to semi-arid and

arid climate in the north. According to the historical data (1975-2005) the average annual rainfall is around 334 mm that changes between 33 mm in summer (8.7 % of total annual rainfall) to 111 mm in spring (34% of total annual rainfall). The rainfall distribution fluctuates between 483 mm in the southeast and 265 mm in the north, as well. Additionally, the average air temperature fluctuates between 7.9-15.2°C which varies between the climate stations based on the location (Tavoosi and Delara, 2010).

Destructive floods events are recurrent natural hazards in the Ardabil Province as it is adjacent to the Caspian Sea. The Ardabil Province crisis management organization data (2016) shows that floods accounts for over a third of disasters in Ardabil Province. Based on statistics, the annually average of flood damages roughly stood around 900,000 USD in the last three years. The total toll by February 2019 flood event was estimated around 370,000 USD (Samani, 2019).

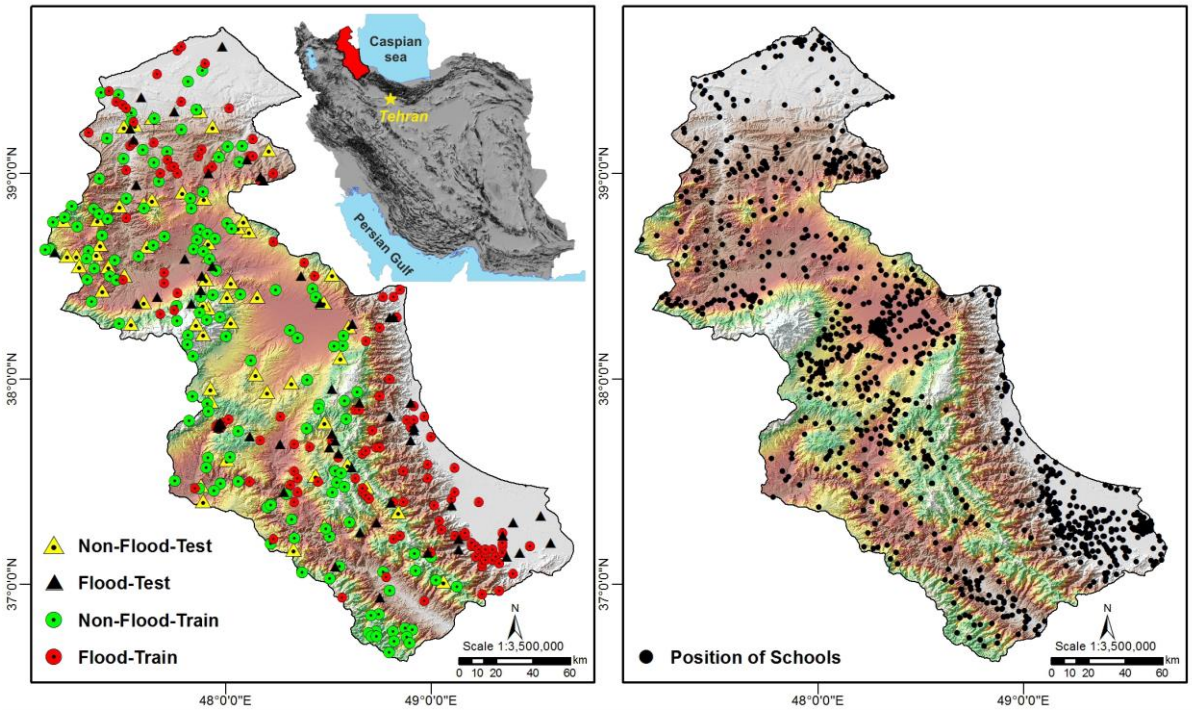

Figure 2. Flood points and school position map of Ardabil province in northwest Iran

3. Methodology

3.1. Data used

138 3.1.1. The Flood inventory map

139 The prerequisite to flood susceptibility spatial modeling is the map of flood inventory
140 which illustrate the historical floods locations. In this study, the map for flood inventory was
141 developed via the 147 flood points identified through the existing reports and verified by field
142 surveys (Figure 2). Figure 3 illustrates some photographs and aerial imagery of the recent
143 flood occurred on 31 March 2019 that occupied several schools. Non-flood points are also
144 identified to be 147 locations. Then, the points were randomly divide into training and testing
145 subsets. According to the literature review, 70% of the points, 103 points, were used to train
146 the models and 30% of them, 44 points, were used for testing the models (Jaafari et al.,
147 2019).

148
149 **Figure 3.** Some photographs and aerial imagery of the recent flood on 31 March 2019 occupied the schools

150 3.1.2. Factors influencing flood

151 Identifying the most effective factors for flood is essential for developing a reliable
152 flood susceptibility map. The impact of flood on influencing factors varies from a region to
153 another with respect to the local hydro-environmental characteristics. Literature and available

154 data revealed that nine flood influencing factors could be selected: altitude, slope, aspect,
155 plan curvature, rainfall, normalized difference vegetation index (NDVI), land use, lithology,
156 and distance from river (Ahmadlou et al., 2021; Shafapour Tehrany et al., 2019; Ullah and
157 Zhang, 2020). Figure 4. Illustrates the selected factors over the study region based on the
158 spatial variability. Input variables were entirely transformed to the raster format with spatial
159 resolution of 30 m in the GIS interface (Esri, Redlands, CA, USA). Following, we briefly
160 describe these factors and their significance on predictive modeling of floods.

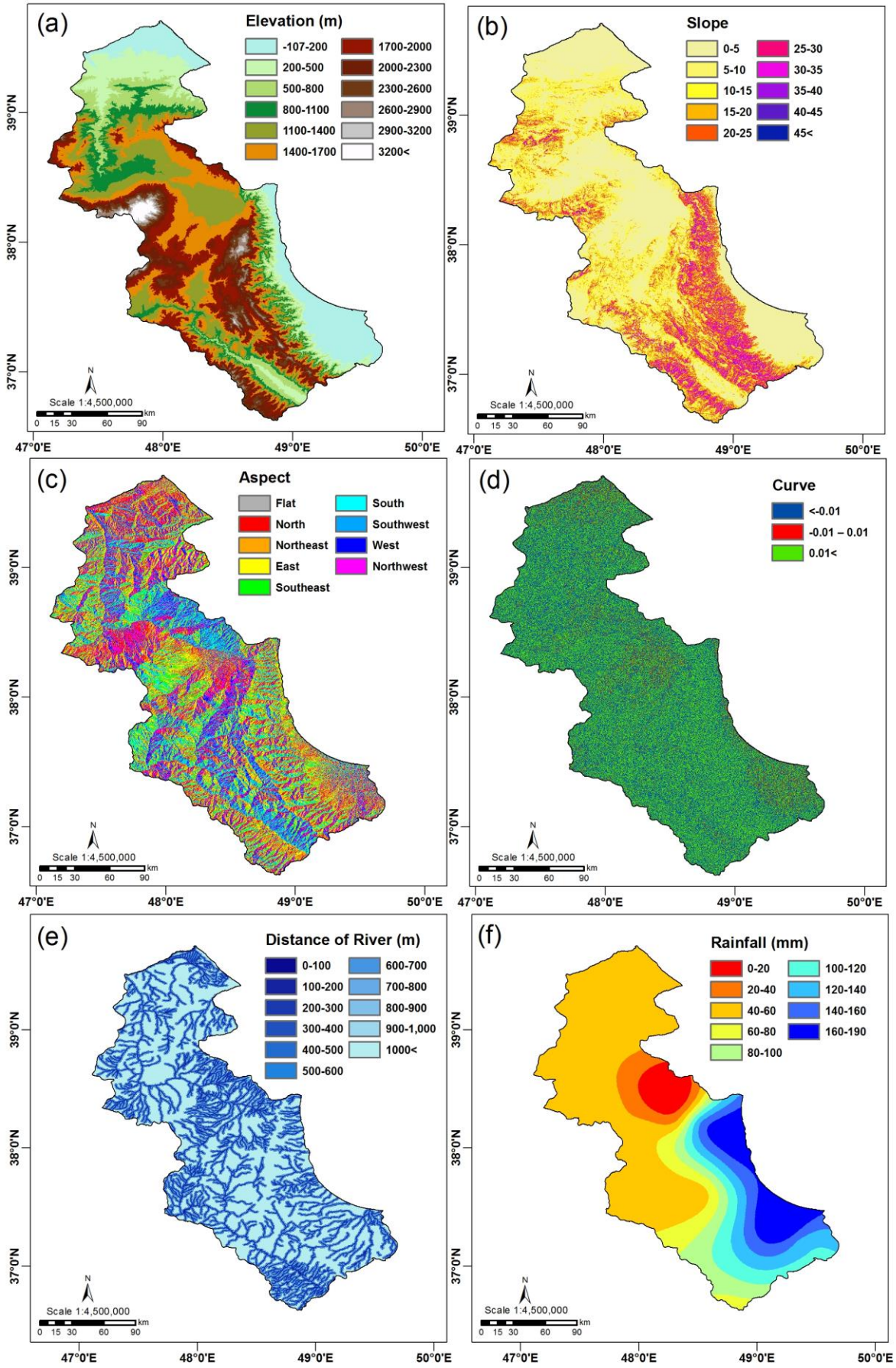

Figure 4. Flood influencing factors used in this study

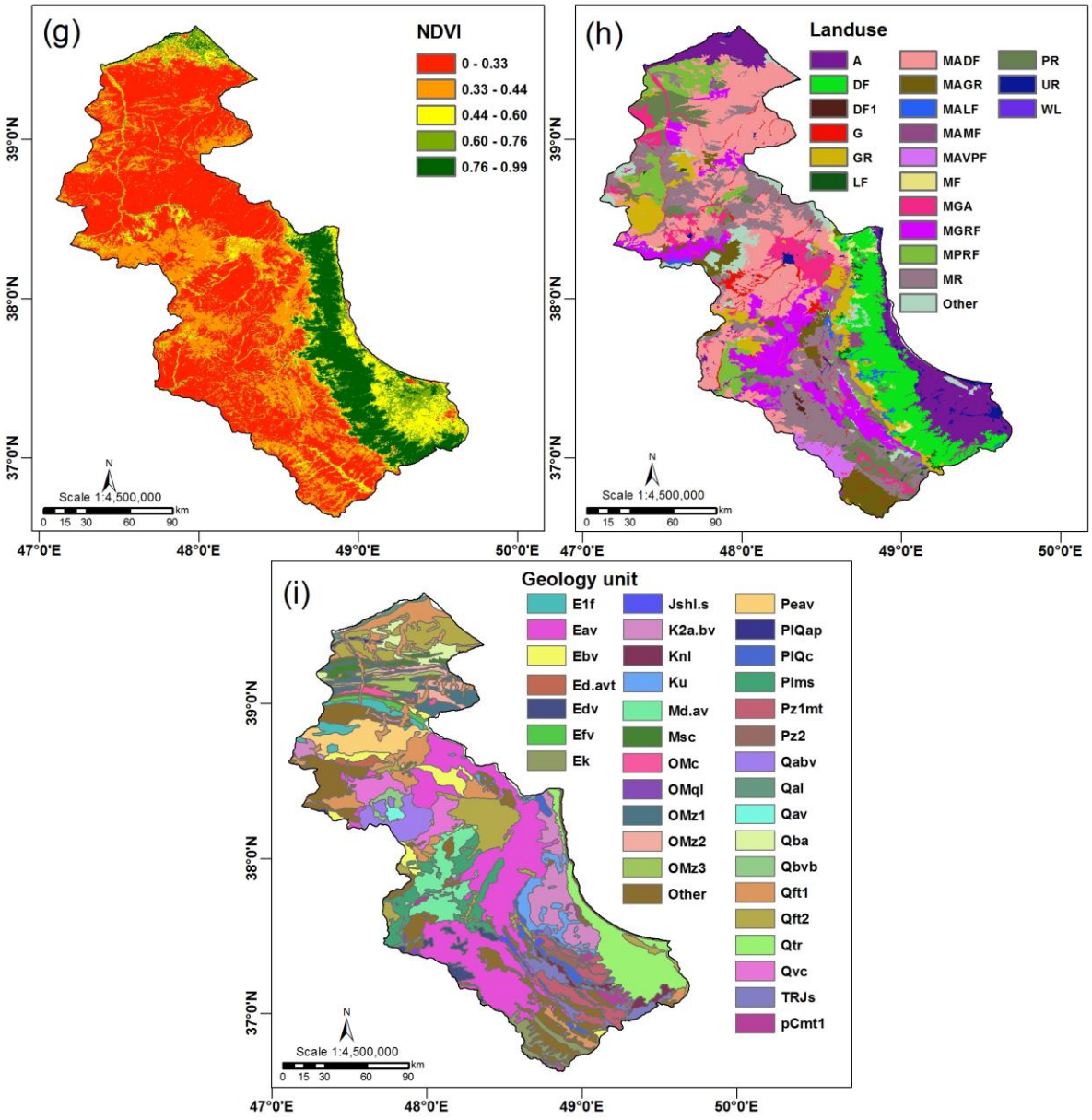

Figure 4. Continued

3.1.2.1. Altitude

Altitude plays an effective role in flood inundation (Allafta and Opp, 2021; Park and Lee, 2020). Altitude is inversely related to the probability of flooding since flooding occurs more in low elevated areas due to the runoff flowing down from higher altitudes (Khosravi et al., 2018). Based on the field surveys and inspection of the flood inventory map (Figure 2), it is revealed that most of the flooding points are distributed within the low elevated hill slopes specifically in the northern hill slopes of the Alborz mountain range. Thus, the digital elevation model (DEM), which was obtained from the U.S. Geology Surveys (USGS)

173 (https://earthexplorer.usgs.gov), is applied in order to drive the altitude map and the next four
174 layers (Figure 4).
175 3.1.2.2. Slope
176 Slope is another factor which has great effects the runoff velocity and volume. The
177 velocity of runoff and volume increase in steep slopes (Khosravi et al., 2016b). Slope has an
178 reverse effect on infiltration rate which means when the slope increases, infiltration rate of
179 runoff decreases and this would cause a great deal of runoff to be generated (Tehrany et al.,
180 2015). The slope gradient is highly variable in the area under study which highest flooding
181 events occurred in the slope gradient > 20-25° so this factor was considered in current study
182 to predict the flood susceptibility. The slope map was developed in 10 classes using the DEM
183 (Figure 4b).
184 3.1.2.3. Aspect
185 Aspect also plays a vital role in studies on flood (Choubin et al., 2019). The areas
186 overlooking the lightning aspects are flooded less occasionally. Yates et al. (2002)
187 demonstrated that the slope aspect greatly affects hydrologic response unit. In the area under
188 study, aspect factor influenced the flooding by conditioning different local climatic
189 conditions in the northern and southern hills of the Alborz Mountain range. The northern hills
190 overlook the Caspian Sea and are more humid than the southern hills which have more
191 potential for flooding. Rahmati et al. (2016) also proved that slope aspect can show local
192 climatic conditions and soil moisture content. The aspect has been categorized in 9 classes in
193 this study, as represented in Figure 4c.
194 3.1.2.4. Plan curvature
195 Curvature is another influencing factor that affects the susceptibility of an area to
196 flood occurrences (Cardenas et al., 2004). Flood occurrence is higher in both concave and flat
197 areas(Tehrany et al., 2015, 2014). Concave slopes are the focal points of runoff and thus have

198 a high potential for flooding. As Figure 2 displays, the topography of the study region is
199 characterized by many concave slopes which encompasses a great number of historical
200 flooding points (Figure 4d).

201 3.1.2.5. Distance from river

202 The risk of flooding is getting higher while a region's distance is getting closer to
203 river which has been proved by Predick and Turner (2008). Additionally, Tien Bui et al.
204 (2018) noticed that most flood events happens in those regions where close to rivers. As
205 Figure 4e depicts, the distance from the rivers is classified into eleven categories that range
206 between 0-100 to > 1000 m. There is a dense drainage network in the southeastern part of the
207 area under study responsible for the transport of runoff to the northern hills of the Caspian
208 Sea. Figure 2 also shows that most of the flooding points are concentrated in this area and
209 along the riverside in other areas.

210 3.1.2.6. Rainfall

211 Another factor which considerable mentioned in the literature and plays a pivotal role
212 in flood susceptibility mapping is rainfall (Breinl et al., 2021; Das and Scaringi, 2021;
213 Sharma et al., 2017). There is a significant association between the rainfall and flooding
214 throughout the area under study. The northern hills of the Alborz Mountain range receive the
215 highest amount of rainfall (Figure 4f) and experienced a great number of flooding events
216 during the past years (Figure 2). In this study, the mean annual rainfall map is used that
217 retrieved from the Iran Meteorological Organization (IRIMO). The annual rainfall was
218 categorized into nine classes with the highest annual rainfall (> 160 mm) in the southeastern
219 coastal regions of the province (Figure 4f).

220 3.1.2.7. Normalized difference vegetation index (NDVI)

221 The NDVI index is applied to assessing the vegetation attributes in a region. Since a
222 negative correlation exists between flooding and vegetation density (Kumar and Acharya,

223 2016; Tehrany et al., 2013), utilization of this index would bear fruitful results in developing
224 the flood susceptibility map. As described in section 3.1.2.3 topography of the region due to
225 the effects of the Alborz Mountains has caused various local climatic conditions over the
226 region. On the northern slopes of these Mountains, vegetation is denser than other areas
227 because of higher moisture content so the NDVI values are calculated as an indicator of
228 vegetation status to predict flood susceptibility. The following equation was applied in order
229 to not only calculate, but also to map the NDVI map of the region under study (Figure 4g)
230 (Tucker and Seller, 1986):

231 $$NDVI = \frac{NIR - R}{NIR + R} \quad (1)$$

232 where R and NIR indicate the red portion of the electromagnetic spectrum (0.63-0.69μm) and
233 the near-infrared portion of it (0.76-0.90μm), respectively. Further, the Landsat 7 Enhanced
234 Thematic mapper plus (ETM+) images, was acquired from the US Geological Survey, were
235 used to develop NDVI map of the study (available at https://esrthyexplorer.usgs.gov, last
236 access: 1 March 2019).

237 3.1.2.8. Land use

238 The usage of land is accounted as an important anthropogenic variables directly
239 affecting velocity and volume of runoff (Yalcin et al., 2011) as well as transportation of
240 sediment (Los Huertos, 2020). Several studies underscored the importance of land use pattern
241 on flooding (e.g., Darabi et al., 2020; Mousavi et al., 2019; Narimani et al., 2021; Yulianto et
242 al., 2020). In the area under study, several types of land uses exist such as thick forest and
243 built up areas that have different impacts on flooding. The dense forest decreases the surface
244 runoff and has a preventive role against the flooding while built-up areas accelerate the
245 flooding by reducing the infiltration capacity. In this study, a produced land use map by the
246 Ministry of Agriculture (Iran) in 2012 was used (Figure 4h).

247 3.1.2.8. Lithology

Lithology undoubtedly plays a part in the volume and speed of runoff through controlling the rate of infiltration as well as transport of sediment. The transport of sediment, itself a flood-related component, is under the influence of geological formation erodibility. In their study, Lee et al. (2012) showed that different units of geology have various susceptibilities to flooding. Lithology greatly influences the hydrological and hydrogeological conditions by controlling the infiltration and surface runoff (Bui et al., 2019) as well as the slope of channel in temporal floods (Waqas et al., 2021; Zzaman et al., 2021). The geology map of study's region consisted of 31 geology units that was obtained from Geology Survey of Iran (https://gsi.ir/fa) as represented in Figure 4i.

3.2. Theoretical background of the used methods

3.2.1. Frequency ratio

Recognizing the conditions for flood occurrence has great importance in evaluation the spatial probability of flood occurrence over time. It can be obtained from the connection between areas without past flood and the flood influencing factors. To statistically investigate this relationship and obtain an initial weight for each subclass of each influencing factor, we used frequency ratio (FR) method. FR method is calculated via distribution of flood locations and each influencing factors. The greater FR value of a certain class from each influencing factor shows the greater importance of the class to occurrence (Shirzadi et al., 2017). Firstly, the FR is computed for subclasses of each influencing factor and then the FRs are summed to obtain the flood susceptibility index (FSI) according to the following equations:

$$FR_{Flood} = \frac{FOR}{AR} \quad (2)$$

$$FSI = \sum^{n} FR_{Flood} \quad (3)$$

where FR_{Flood} is the frequency ratio for subclasses of each influencing factor, FOR is the flood occurrence ratio, AR represents the area ratio, and n shows the number of flood influencing factors.

3.2.2. Support vector regression (SVR)

SVR can be considered as a class of controlled machine learning algorithms which can be used as a prediction model and a applicable tool for solving pattern recognition problems (Vapnik, 1995). In this algorithm, for a given training data samples $x=(x_1, x_2, ..., x_n)$; the predicted values ($y_i \in R^n$) can be computed through a linear approximation function (f(x)). The accuracy of the process can be determined by the ε-deviation value which calculates the deviations of the outputs from all corresponding pairs of training sets. The relationship between inputs-outputs data can be expressed as the following:

$$f(x) = w\varphi(x) + b \tag{4}$$

where $w \in R^n$, $b \in R$, and n are weight factor, bias vector and the number of training data samples, respectively. In addition, $\varphi(x)$ is a non-linear transfer function applied to map the linear/non-linear original input dataset to the higher dimensional feature space. With the aim of enhancing the smoothness and simplicity of the SVR model, w is selected as small as possible (İskenderoğlu et al., 2020; Yu et al., 2006). Based on theory of structural risk minimization, w and b can be determined by the following formula:

$$\text{Minimize}: \left[\frac{1}{2}\|w\|^2 + C\sum_{i=1}^{n}(\xi_i + \xi_i^*)\right] \qquad \text{Subject to:} \begin{cases} y_i - (w\varphi(x_i) + b_i) \le \varepsilon + \xi_i \\ (w\varphi(x_i) + b_i) - y_i \le \varepsilon + \xi_i^* \\ \xi_i, \xi_i^* \ge 0 \end{cases} \tag{5}$$

where C f 0 is the regularization parameter which influences the accuracy of the model; thus small forecasting error can be ensured if C be selected big enough. On the other hand, this parameter can affect the flatness of the SVR function. ξ_i, ξ_i^* are the slack variables which

minimize the objective function. The function of support vector regression can be formulated as follows (Su et al., 2018).

$$f(x) = \sum_{i=1}^{n} (\alpha_i - \alpha_i^*) k(x, x_i) + b \quad (6)$$

where α_i, α_i^* are Lagrange coefficient and $k(x, x_i) = \langle \varphi(x), \varphi(x_i) \rangle$ stands for kernel functions like polynomial, sigmoid, linear, and radial basis function (RBF) (Mohammadi and Mehdizadeh, 2020). RBF is the optimal kernel function (Huang et al., 2020) which leads to shortening calculation time and increasing prediction accuracy (Yao et al., 2018) Since in this study RBF is used; Eq. (3) can be revised as follows:

$$f(x) = \sum_{i=1}^{n} (\alpha_i - \alpha_i^*) \exp\left(\frac{-\|x - x_i\|^2}{2\sigma^2}\right) + b \quad (7)$$

where σ is the parameter of the RBF. The detailed information of the SVR model and its applications in different scientific fields can be pursued in (Alade et al., 2019; Hamed et al., 2020; Owolabi, 2019; Panahi et al., 2020; Shahsavar et al., 2019).

3.2.3. Meta-optimization algorithms

Traditional SVR learning is based on the gradient descent algorithm which uses the slow convergence and inefficient solutions to gain the optimized values for ε, C and σ (Cetisli and Edizkan, 2011). In current research, two meta-heuristic optimization algorithms, i.e. GWO and WOA were applied to optimizing the SVR model. The GWO algorithm has superior exploitation capability and high local avoidance compared to the other meta-heuristic algorithms such as Gravitational Search Algorithm (GSA), Differential Evolution (DE), Partial Swarm Optimization (PSO), Evolutionary programming (EP), Evolution Strategy (ES), etc. (Mirjalili et al., 2014). The WOA algorithm requires fewer number of function evaluations in comparison with other meta-heuristic algorithms for finding the best

optimal design (Mirjalili and Lewis, 2016). Thus, we employed these algorithms to train the SVR model so as to improve the model's predictive accuracy.

3.2.3.1. Whale optimization algorithm (WOA)

This algorithm innovated by Mirjalili and Lewis (2016) to manage the optimization problems. WOA algorithm theory was inspired by the bubble net feeding behavior of Humpback whales (Watkins and Schevill, 1979). The bubbles along the circles created by Humpback whales which enable them to chase and eat tiny fishes and other marine creature. In this algorithm, situation of the Humpback whales around the best solution is formulated as follow (Mirjalili and Lewis, 2016):

$$\vec{X}(t+1) = \vec{X}^{*}(t) - \vec{A}.\left|\vec{C}.\vec{X}^{*}(t) - \vec{X}(t)\right| \quad (8)$$

where $\vec{X}$ is the situation vectors of the Whale, t shows the running iteration, X^* denotes the situation vector of the best solution and if there was a better solution it would be updated, $\vec{A} = 2\vec{a}.\vec{r} - \vec{a}$ and $\vec{C} = 2.\vec{r}$ represent coefficient vectors and as iterations proceed, $\vec{a}$ is decreasing linearly from 2 to 0. $\vec{r}$ indicates a random vector takes a value between [0,1].

The Bubble-net attacking approach contains: i) shrinking encircling movement which is represented through the dimensioning $\vec{a}$ in $\vec{A} = 2\vec{a}.\vec{r} - \vec{a}$ formula. The value of $\vec{A}$ is also decreases while $\vec{a}$ is decreasing. ii) Spiral updating position used to modeling the whale's spiral movement around the hunt by computing the position of the hunt (X^*, Y*) to the hunter (X, Y):

$$\vec{X}(t+1) = \vec{D}'e^{bl}.\cos(2\pi l) + \vec{X}^{*}(t) \quad (9)$$

where $\vec{D}' = \left|\vec{X}^{*}(t) - \vec{X}(t)\right|$ stands for the space between the prey and i-*th* predator. b represents a fixed value which determines the logarithmic helix-shaped motions, l randomly varies between [-1,1]. The whale's motion in the periphery of the prey is along with the

spiral-shaped paths by shrinking the circles. The mathematical modeling of these kind of behaviors can be shown in the following (Mirjalili and Lewis, 2016):

$$\vec{X}(t+1)=\begin{cases}\vec{X}^{*}(t)-\vec{A}.\vec{D} & if \quad p<0.5\\ \vec{D}'.e^{bl}.\cos(2\pi l)+\vec{X}^{*}(t) & if \quad p\geq 0.5\end{cases} \tag{10}$$

where p∈ [0,1] explains the probability of either maintaining the rotation mode or taking a shrinking encircling to updating their situations. In the searching phase (exploration), the whales tracking the hunt in a random mode according to the situation of each other (Mirjalili and Lewis, 2016). Therefore, the situations of whales will be updated based on randomly selected searching factor in place of the best searching factor:

$$\vec{D}=\left|\vec{C}.\vec{X}_{rand}-\vec{X}\right| \tag{11}$$

$$\vec{X}(t+1)=\vec{X}_{rand}-\vec{A}.\vec{D} \tag{12}$$

where $\vec{X}_{rand}$ explains a random situation derived from the current population. Detailed information on this algorithm can be found in Mirjalili and Lewis (2016).

3.2.3.2. Grey wolf optimizer (GWO)

This algorithm (Mirjalili et al., 2014) is another nature-inspired algorithm that mimic the social hierarchy of wolves as well as their behavior during approaching, encircling, and attacking the prey (Faris et al., 2018). Each member in a grey wolf herd classified as omega (ω), delta (δ), beta (β), and alpha (α) based on their effectiveness and power to making decisions in the herd. The strongest and dominant wolf is α who leads the herd and his/her order is compulsory for the rest of the group members (Mech, 1999). The second place belongs to β wolves that they play the role of advisors for α (Mirjalili et al., 2014). The α wolves reinforce their commands to the rest of wolves by the help of the β wolves (Mirjalili et al., 2014; Yue et al., 2020). Based on the leadership hierarchy, the lowest rank belongs to ω wolves and above them are δ wolves. The δ wolves are hunters, sentinels, guards, and caretakers of the group (Jaafari et al., 2019). The ω wolves have to submit to all other wolves.

In a hunting process, the grey wolfs track, encircle and attack the hunt in sequential stages (Muro et al., 2011). The hunting process is arranged by α, β, and δ wolves, and the ω wolves follow them (Mirjalili et al., 2014). The best solution to optimizing the problem is α. The β, δ, and ω comes after α, respectively, in term of priority. The encircling process can be defined as the following (Mirjalili et al., 2014):

$$\vec{X}(t+1) = \vec{X}_p(t) - \vec{A}.\left|\vec{C}.\vec{X}_p(t) - \vec{X}(t)\right| \quad (13)$$

where $\vec{X}_p$ and $\vec{X}$ are the position vectors of the hunt and hunter, respectively (candidate solutions), t is the current iteration, and $\vec{A} = 2\vec{a}.\vec{r}_1 - \vec{a}$ and $\vec{C} = 2.\vec{r}_2$ are coefficients vector with $\vec{r}_1$ and $\vec{r}_2$ $\in[0,1]$ as random vectors that allow the wolves update their situation according to the hunt space. $\vec{a}$ are linearly reduced from 2 to zero during the process as follow:

$$a(t) = 2 - \frac{2t}{\sum t} \quad (14)$$

where $\sum t$ is the total number of iterations and t shows the current iteration. During the search process, ω wolves update their location according to the best exploration factors i.e., α, β, and δ location expressed by the following equations (Mirjalili et al., 2014):

$$\vec{X}_1 = \vec{X}_\alpha - \vec{A}_1.\left|\vec{C}_1.\vec{X}_\alpha - \vec{X}\right| \quad (15)$$

$$\vec{X}_2 = \vec{X}_\beta - \vec{A}_2.\left|\vec{C}_2.\vec{X}_\beta - \vec{X}\right| \quad (16)$$

$$\vec{X}_3 = \vec{X}_\delta - \vec{A}_3.\left|\vec{C}_3.\vec{X}_\delta - \vec{X}\right| \quad (17)$$

$$\vec{X}(t+1) = \frac{\vec{X}_1 + \vec{X}_2 + \vec{X}_3}{3} \quad (18)$$

3.3. Evaluation and comparison of the models

The receiver operating characteristic (ROC) technique was applied to evaluate the hybrid SVR- models. The ROC curve as a two-dimensional curve with true-positive rates

(sensitivity) on x-axis versus false-positive rates (100-specificity) on the y-axis has been proposed and employed to evaluate the flood predictive models (Ali et al., 2020; Arabameri et al., 2021a; Norallahi and Seyed Kaboli, 2021; Pourghasemi et al., 2020; Schumann et al., 2014). The sensitivity is defined as the number of occasions which flooded pixels are correctly distinguished as flooded and the specificity as the frequency of non-flooded pixels distinguished as non-flooded area (Gudiyangada Nachappa et al., 2020). The region which is under the ROC curve (AUC) is applied to quantitatively assess the developed hybrid model. The values of AUC ranges between 0 and 1 where the model is absolutely non-informative or absolutely performed well, respectively (Kalantar et al., 2021; Yariyan et al., 2020). When the value of AUC increases, the model becomes better (Fawcett, 2006). The AUC's values classified as four category, i) poor model performance, less than 0.6; , ii) moderate model performance, 0.6 - 0.7, iii) good model performance, 0.7 -0.8, and iv) very good model performance is above 0.8. The performance of the developed models is also assessed with respect to the statistical goodness-of-fit criteria such as mean absolute error (MAE) and root mean square error (RMSE).

4. Results and discussion

4.1. Spatial relationship of flood and influencing factors by using FR model

Although there are certain influencing factors affecting flood events, contribution of each factor and pertaining sub-categories varies from region to region (Fernández and Lutz, 2010). If the most influencing factors in relation to the hydro-environment characteristics were selected properly, the predictive performance of the models can be effectively improved reproducing the flood susceptibility maps (Khosravi et al., 2018; Nguyen et al., 2021). To this end, the FR method was used to determine the contribution of each natural environmental factor to flooding. The weights of each flood influencing factors and pertaining subclasses are provided in Table 1. The higher values of FR weight is (> 1), the stronger connection

happens between the flood occurrence and flood influencing factors. The FR weights identical to 1 represent the average connection and the values less than 1 represents the weak connection between the factors affecting flood and the occurrence of flood (Pradhan, 2010; Rahmati et al., 2016). From Table 1, it is seen that all of the influencing factors have remarkably influenced the flooding. The use of land and lithology are among the most effective factors. NDVI, rainfall, and altitude were ranked in the next orders. The result concurs with Hong et al. (2018) and Rahman et al. (2021) findings who acknowledged the significant role of lithology and land use on flood occurrence. The importance of lithology, land use, and altitude was also highlighted by Rahmati et al. (2016). Tien Bui et al. (2016) emphasized the high predictive utility of NDVI in spatial prediction floods, which supports the results of our study. For the investigation of the role of the land use schemes on flood occurrence, the association of different land use types with the frequency of flood event points was measured. The results indicated that dry farming lands with highest FR weight (7.07) as well as the mixed gardens and agricultural lands with FR weight of 3.66 were areas with the highest susceptibility to flooding. The rangelands, on the other hand, were less susceptible to flooding with the lowest FR value of 0.18. The areas with altitude of -107 - 200 m above the mean sea level have the highest FR weight (2.12) indicating the highest susceptibility of flooding in these regions. This is the reason that the agricultural lands are more exposed to flooding and rangelands are less likely. Because agricultural lands spread along the low-lying areas, while the rangelands spread at high altitudes.

Table 1. FR weights for sub-classes of flood influencing factors

Flood influencing factor	Class	No. of pixels in domain	Percentage of domain	No. of flood	Percentage of flood	Weight FR
Altitude (meter)	-107 - 200	551004	0.13	37	0.27	2.12
	200-500	398896	0.09	22	0.16	1.74
	500-800	373004	0.09	10	0.07	0.85

	800-1100	411285	0.09	15	0.11	1.15
	1100-1400	719670	0.17	12	0.09	0.53
	1400-1700	713360	0.16	19	0.14	0.84
	1700-2000	545479	0.13	17	0.12	0.98
	2000-2300	337965	0.08	4	0.03	0.37
	2300-2600	173103	0.04	2	0.01	0.36
	2600-2900	77472	0.02	0	0.00	0.00
	2900-3200	23875	0.01	0	0.00	0.00
	3200<	28834	0.01	0	0.00	0.00
Slope (angle)	0-5	1747842	0.40	56	0.41	1.01
	5-10	803218	0.18	18	0.13	0.71
	10-15	585559	0.13	26	0.19	1.40
	15-20	442394	0.10	18	0.13	1.28
	20-25	344850	0.08	12	0.09	1.10
	25-30	251574	0.06	5	0.04	0.63
	30-35	137269	0.03	3	0.02	0.69
	35-40	35302	0.01	0	0.00	0.00
	40-45	4905	0.00	0	0.00	0.00
	45<	1034	0.00	0	0.00	0.00
Aspect	Flat (-1)	6281	0.00	0	0.00	0.00
	North	609873	0.14	23	0.17	1.19
	Northeast	618019	0.14	18	0.13	0.92
	East	613277	0.14	22	0.16	1.13
	Southeast	559783	0.13	13	0.09	0.73
	South	456782	0.10	20	0.14	1.38
	Southwest	439525	0.10	15	0.11	1.08
	West	479967	0.11	9	0.07	0.59
	Northwest	570440	0.13	18	0.13	1.00
Curvature (100/m)	<-0.01	2016906	0.46	67	0.49	1.05
	-0.01 – 0.01	187012	0.04	10	0.07	1.69
	0.01<	2150029	0.49	61	0.44	0.90
Distance of River (meter)	0 - 100	100	269594	0.05	15	0.11
	100 - 200	200	265405	0.05	14	0.10
	200 - 300	300	258436	0.05	17	0.12

	300 - 400	400	251734	0.05	15	0.11
	400 - 500	500	244733	0.05	7	0.05
	500 - 600	600	236429	0.05	4	0.03
	600 - 700	700	226709	0.05	6	0.04
	700 - 800	800	215970	0.04	5	0.04
	800 - 900	900	204340	0.04	4	0.03
	900 - 1000	1000	193103	0.04	7	0.05
	1000 <	9999	2572067	0.52	44	0.32
Rainfall (mm)	0-20	187619	0.04	3	0.02	0.50
	20-40	212359	0.05	0	0.00	0.00
	40-60	2084206	0.48	60	0.43	0.91
	60-80	281411	0.06	4	0.03	0.45
	80-100	327639	0.08	7	0.05	0.67
	100-120	312874	0.07	9	0.07	0.91
	120-140	312771	0.07	19	0.14	1.92
	140-160	271861	0.06	19	0.14	2.20
	160-190	363040	0.08	17	0.12	1.48
NDVI	0 - 0.33	289331	0.49	34	0.25	0.50
	0.33 - 0.44	150485	0.26	35	0.25	0.99
	0.44 - 0.60	47236	0.08	26	0.19	2.33
	0.60 - 0.76	36311	0.06	16	0.12	1.87
	0.76 - 0.99	61594	0.11	27	0.20	1.86
Geology	E1f	68859	0.01	2	0.01	1.03
	Eav	867007	0.18	11	0.08	0.45
	Ebv	113622	0.02	2	0.01	0.63
	Ed.avt	23316	0.00	1	0.01	1.53
	Edv	51967	0.01	2	0.01	1.37
	Efv	24918	0.01	1	0.01	1.43
	Ek	78150	0.02	1	0.01	0.46
	Jshl.s	24029	0.00	1	0.01	1.48
	K2a.bv	239298	0.05	10	0.07	1.49
	Knl	43224	0.01	2	0.01	1.65
	Ku	102422	0.02	4	0.03	1.39
	Md.av	170859	0.03	11	0.08	2.29

	Msc	50739	0.01	2	0.01	1.40
	OMc	25930	0.01	2	0.01	2.74
	OMql	6619	0.00	1	0.01	5.37
	OMz1	111377	0.02	7	0.05	2.24
	OMz2	66658	0.01	1	0.01	0.53
	OMz3	57368	0.01	3	0.02	1.86
	Other	544374	0.11	0	0.00	0.00
	pCmt1	35584	0.01	5	0.04	5.00
	Peav	159441	0.03	1	0.01	0.22
	Plms	186329	0.04	5	0.04	0.95
	PlQap	5706	0.00	1	0.01	6.23
	PlQc	56317	0.01	2	0.01	1.26
	Pz1mt	148124	0.03	9	0.07	2.16
	Pz2	22455	0.00	2	0.01	3.17
	Qabv	113291	0.02	1	0.01	0.31
	Qal	29349	0.01	2	0.01	2.42
	Qav	13822	0.00	1	0.01	2.57
	Qba	67198	0.01	3	0.02	1.59
	Qbvb	24342	0.00	1	0.01	1.46
	Qft1	384592	0.08	2	0.01	0.18
	Qft2	406509	0.08	4	0.03	0.35
	Qtr	318963	0.06	25	0.18	2.79
	Qvc	127740	0.03	2	0.01	0.56
	TRJs	113978	0.02	8	0.06	2.50
Landuse	Agriculture (A)	403125	0.09	28	0.2	2.19
	Dense forest (DF)	434105	0.1	28	0.2	2.03
	Dry farming (DF1)	4451	0	1	0.01	7.07
	Good rangeland (GR)	4451	0	1	0.01	7.07
	Low forest (LF)	225972	0.05	2	0.01	0.28
	Mixture of garden and agriculture (MGA)	18830	0	1	0.01	1.67
	Mixture of agriculture with dry farming (MADF)	214261	0.05	10	0.07	1.47
	Garden (G)	79709	0.02	3	0.02	1.18

Mixture of agriculture with dry farming (MADF)	17201	0	2	0.01	3.66
Mixture of agriculture and good rangeland (MAGR)	17201	0	2	0.01	3.66
Mixture of agriculture and low forest (MALF)	855128	0.2	23	0.17	0.85
Mixture of agriculture and Moderate forest (MAMF)	171307	0.04	1	0.01	0.18
Mixture of good rangeland and fallow (MGRF)	30323	0.01	1	0.01	1.04
Mixture of Poor range and fallow (MPRF)	25212	0.01	2	0.01	2.5
Mixture of agriculture and and very poor forest (MAVPF)	383530	0.09	6	0.04	0.49
Woodland (WL)	222469	0.05	3	0.02	0.42
Moderate forest (MF)	56723	0.01	1	0.01	0.55
Moderate range (MR)	101489	0.02	1	0.01	0.31
Other	35964	0.01	2	0.01	1.75
Poor range (PR)	707913	0.16	15	0.11	0.67
Urban and residential (UR)	92275	0.02	0	0	0
Agriculture (A)	222866	0.05	7	0.05	0.99
Dense forest (DF)	40576	0.01	1	0.01	0.78

4.2. Application of SVR to construct ensemble models

In this study, initial weights were obtained based on the SVR model from the FR analysis that this model was called as hybrid FR-SVR (FS) model. Then, two meta-heuristic optimization algorithms were applied to this model to develop two other hybrid models called as FR-SVR-GWO (FSG) and FR-SVR-WOA (FSW). All ensemble models were formulated using the programming language of MATLAB 8.00, in which they were processed and designed by training and validation/testing datasets. During the modeling process and in

436 order to detect the relationship between the FSI values and flood values (1) as well as non-
437 flood (0) locations, these hybrid models were carried out by training dataset. Consequently,
438 the testing dataset was used for assessing the evaluation process of the models. Basically,
439 flood and non-flood areas were divided into 70% for training datasets and 30% for validation
440 process datasets. The result of model construction and validation are given in Figures 5-7. In
441 this study, some statistical metrics including MSE, RMSE, Mean, and StD were computed to
442 assess the goodness of fit as well as performance of the hybrid models. According to the
443 Figures 5a-f, in the training phase of the hybrid FR-SVR model, these values were $2.8268e^{-15}$,
444 $5.3168e^{-8}$, $4.8038e^{-9}$, and $5.3078e^{-8}$, respectively. While for validation phase these values
445 were 0.0672, 0.2593, 0.01446, and 0.2604, respectively. The hybrid FR-SVR-GWO model
446 results showed that the MSE, RMSE, Mean, and StD values based on the training dataset
447 were 0.035, 0.1885, $42.1789e^{-6}$, and 0.1889, respectively. However, for the validation dataset
448 these values were 0.0394, 0.1986, 0.0461, and 0.19433, respectively (Figure 6). Finally,
449 results for the hybrid FR-SVR-WOA model depicted that values of 0.0406, 0.2016, 0.0012,
450 and 0.2021 were achieved by training dataset respectively for MSE, RMSE, Mean, and StD.
451 However, based on the validation dataset, these values were 0.0410, 0.2025, 0.0234, and
452 0.2023, respectively (Figure 7). It is worth noting that the predictive performance of a model
453 is judged based on the testing dataset (Ahmadlou et al., 2018). The lower the metrics error
454 obtained by testing dataset of a model, the higher the accuracy and performance of the model
455 can be achieved (Arabameri et al., 2021b; Chen et al., 2019; Shafizadeh-Moghadam et al.,
456 2018). Therefore, based on the MSE and RMSE error metrics, results indicated that the
457 hybrid FSG model was outperformed the hybrid FSW and FS models, respectively, for flood
458 modeling in the area under study.

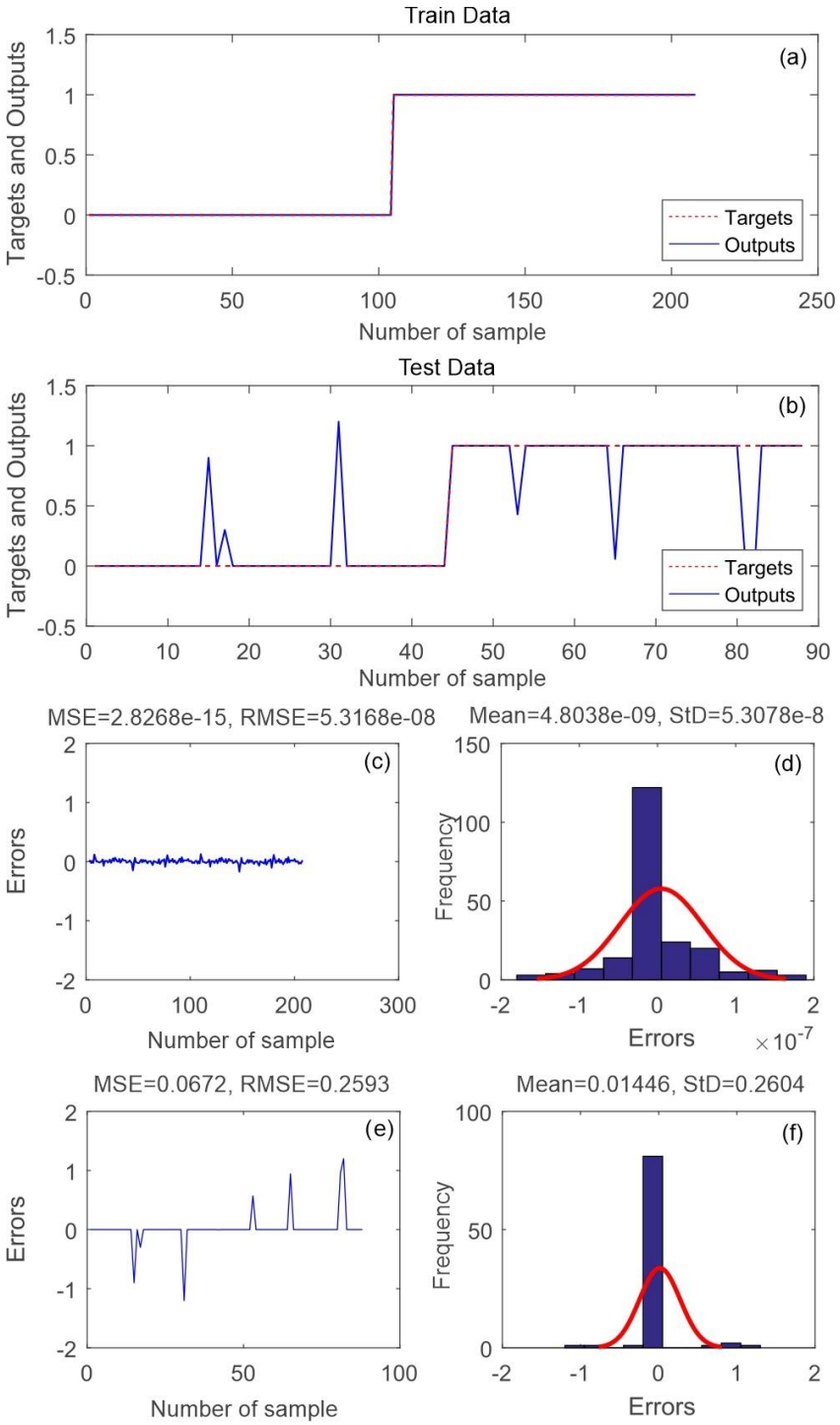

Figure 5. FR-SVR model training and validation results: a) FR-SVR output *vs*. target data for train data samples b) FR-SVR output *vs.* target data for test data samples c) MSE and RMSE values of train data samples d) frequency error of the train data samples e) MSE and RMSE values of test data samples f) frequency error of the test samples

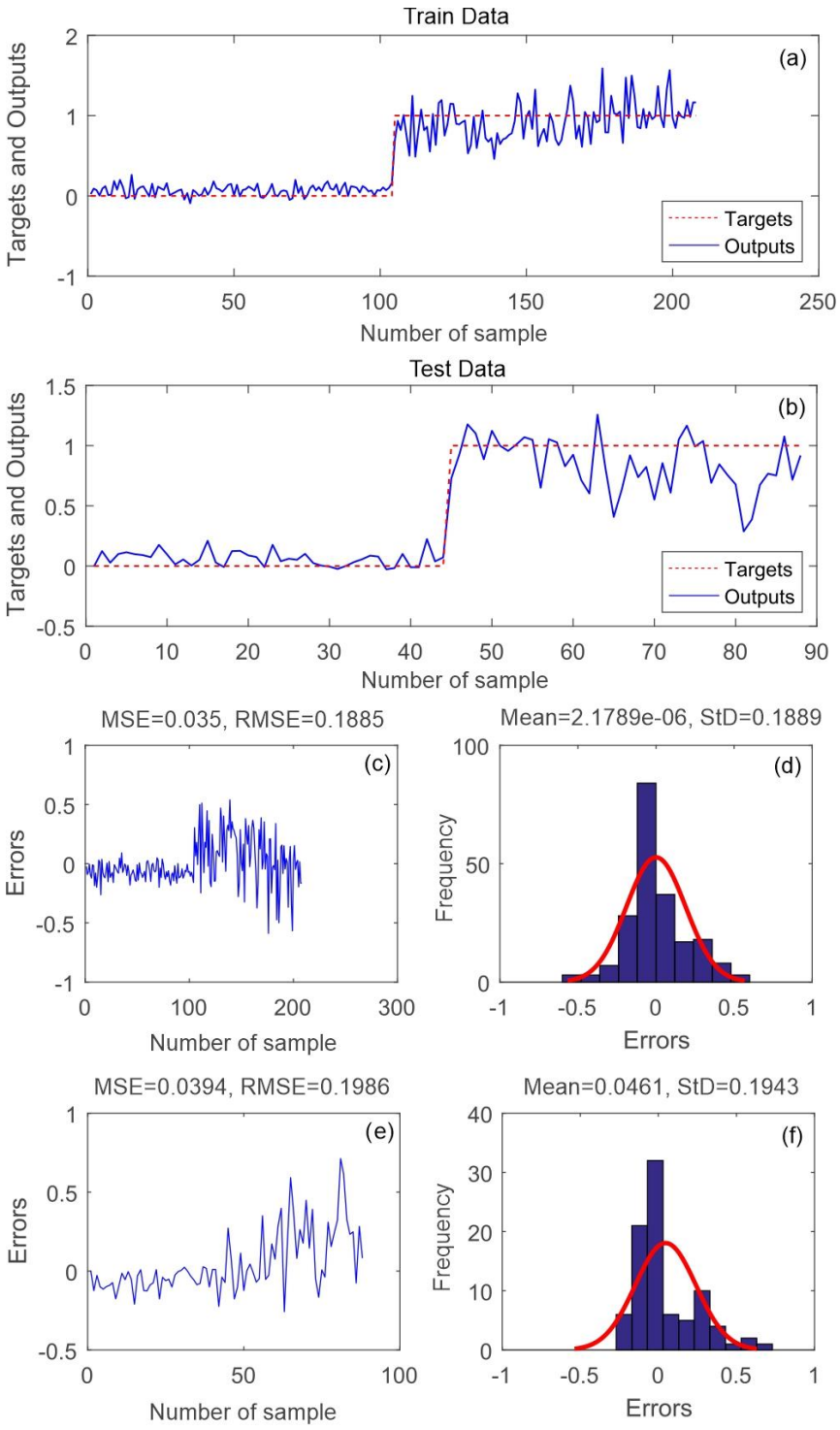

Figure 6. FR-SVR-GWO model training and validation results: a) FR-SVR-GWO output *vs*. target data for train data samples b) FR-SVR-GWO output *vs*. target data for test data samples c) MSE and RMSE values of train data samples d) frequency error of the train data samples e) MSE and RMSE values of test data samples f) frequency error of the test samples

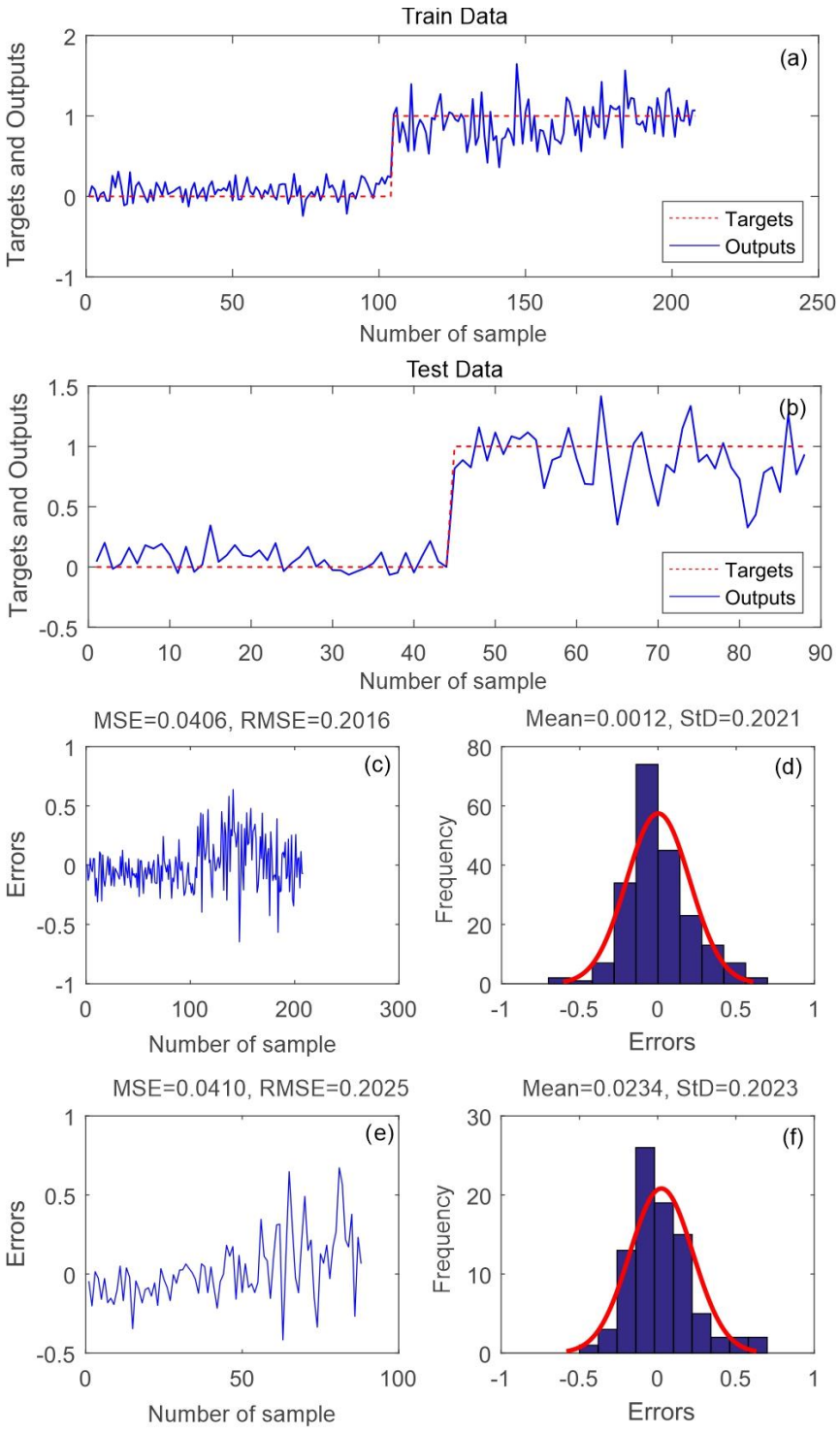

Figure 7. FR-SVR-WOA model training and validation results: a) FR-SVR-WOA output *vs*. target data for train data samples b) FR-SVR-WOA output *vs.* target data for test data samples c) MSE and RMSE values of train data samples d) frequency error of the train data samples e) MSE and RMSE values of test data samples f) frequency error of the test samples

4.3. Comparison and Validation of new hybrid flood susceptibility models

475 At the final stage, for the fulfillment of the FSMs production, four models namely FR,
476 FR-SVR, FR-SVR-GWO, and FR-SVR-WOA were developed using the FR weights and
477 train data sets. For the FR-SVR-GWO and FR-SVR-WOA hybrid models, GWO and WOA
478 optimization algorithms were utilized to optimize the FR-SVR model parameters. The
479 developed models were calibrated via the training data sets and then the calibrated models
480 were utilized to simulating the flood susceptibility index (FSI) for each pixel over the entire
481 study area. Figure 8 shows the convergence speed of the WOA and GWO algorithms. As it is
482 clear from this figure, the GWO algorithm has a higher convergence speed compared to
483 WOA algorithm implying that the GWO algorithm is well suited for application in large
484 scales.

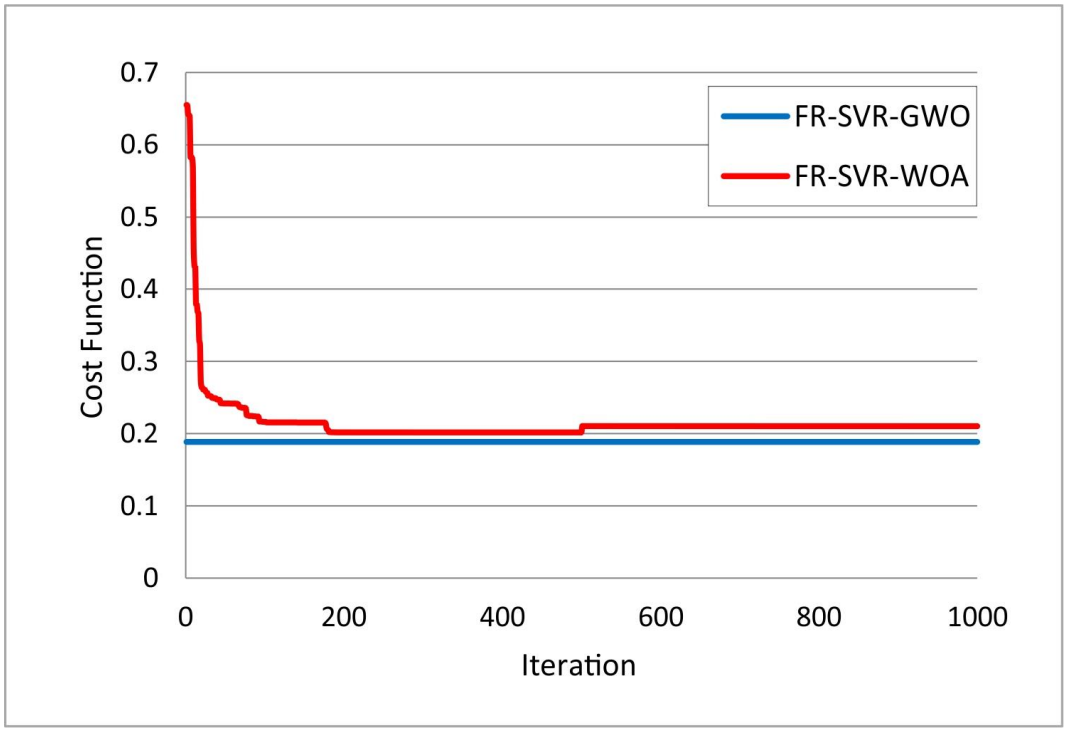

485

486 **Figure 8.** Convergence curves of the developed models

487 The FSI values were classified into five categories via the natural break classification
488 method (Jenks, 1967) to display very high, high, moderate, low, and very low flood
489 susceptibilities areas. By applying this classification method the variance of the data (FSI
490 index here) is minimized and maximized respectively within and between the classes

(McMaster, 1997). Four FSMs were generated in ArcGIS interface based on the reclassified FSI values previously reproduced by the FR, FR-SVR, FR-SVR-GWO, and FR-SVR-WOA models. Figures 9a-d displays the output maps of the four investigated models. On the maps, areas marked in red represent high risk areas for flood occurrence. As it is clear, the coastal areas along the Caspian Sea are the most susceptible areas to flooding. Table 2 shows that the results of the FR-SVR model skewed to the lower and upper tails as the very low and very high susceptibility classes cover the largest percent (very low: 55% and very high: 41%). The FR and FR-SVR-GWO models are similar regarding frequency distribution of the susceptibility classes. For both of these models, the areas with very low and very high susceptibility rates cover the largest (FR model: 40% and FR-SVR-GWO: 45%) and smallest (FR: 8% and FR-SVR-GWO: 2%) percent respectively. For the FR-SVR-WOA the frequency distribution of different susceptibility classes is more uniform than those of the other models. For this model the frequency distribution of the susceptibility classes is as follow: 8% for very high, 15% for high, 16% for moderate, 33% for low, and 28% for very low. The WOA algorithm reproduces greater FSI values comparing to the GWO algorithm. As shown in Figs. 9c-d, by comparing the WOA algorithm and GWO algorithm, the extent of the high and very high susceptibility classes is larger in GWO algorithm. When the goal of flood susceptibility mapping is for reducing the casualties, the WOA algorithm is preferable.

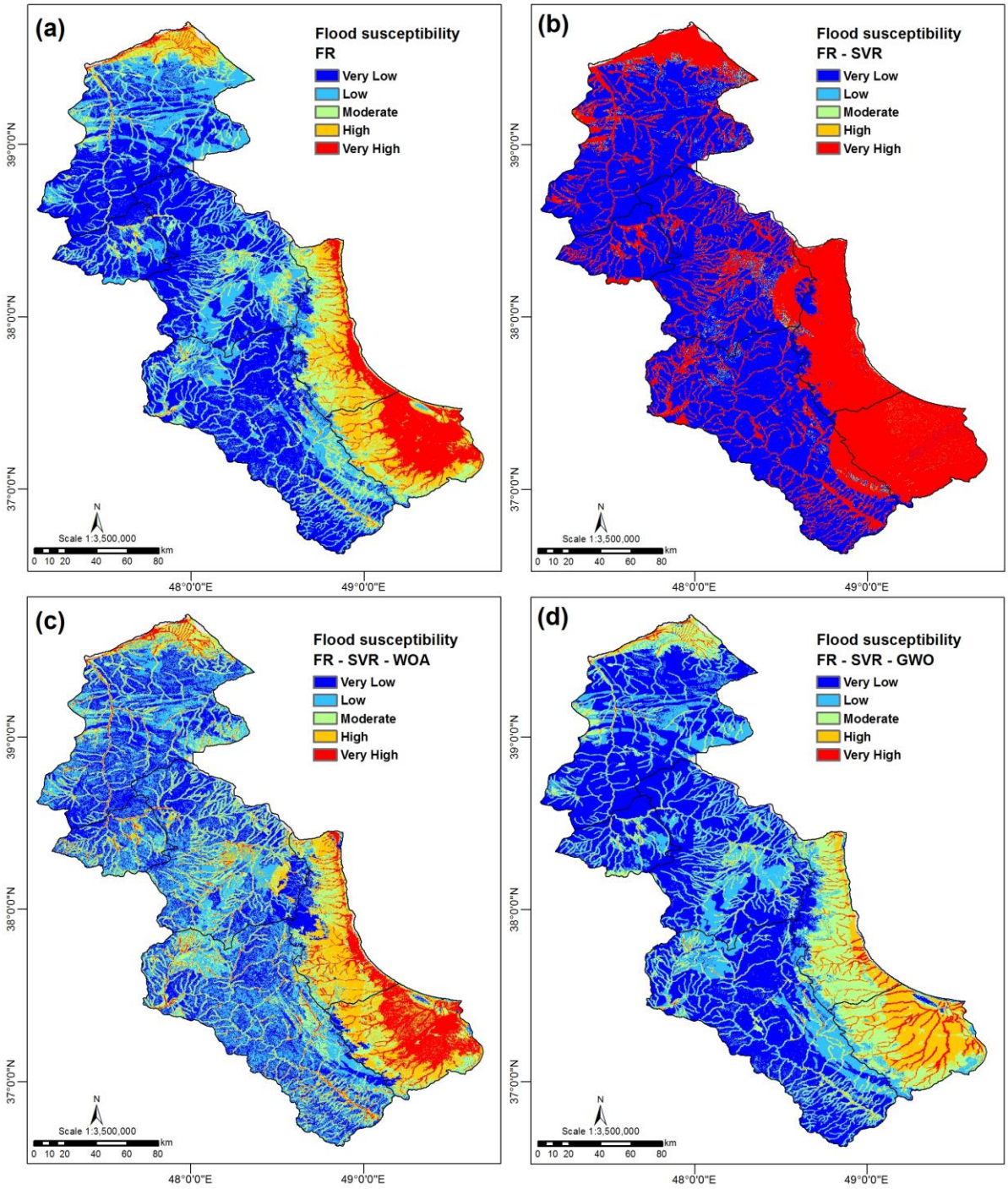

Figure 9. FSMs using (a) FR model, (b) FR-SVR model, (c) FR-SVR-WOA model, (d) FR-SVR-GWO model

Table 2. Percentage of Area reproduced for each flood susceptibility class

Susceptibility rate	FR	FR-SVR	FR-SVR-WOA	FR-SVR-GWO
Very low	40	55	28	45
Low	27	2	33	26

Moderate	14	1	16	18
High	11	1	15	9
Very high	8	41	8	2

512 **4.4. Validation of the proposed hybrid models**

513 The ROC curves were employed to assess the models for FSMs construction. Figures
514 10a-b shows the developed models ROC curves in the training and validation phases. In
515 training phase, the FR-SVR-GWO model enjoys the highest value of AUC, 0.88, and after
516 that the FR-SVR-WOA model (AUC = 0.87) comes. In validation phase, both of the FR-
517 SVR-WOA and FR-SVR-GWO models have the same AUC values (AUC = 0.87) followed
518 by the FR (AUC = 0.84) and FR-SVR (AUC = 0.82) models, indicating their higher
519 performance of the hybrid models. Given the equal AUC values for the FR-SVR-WOA and
520 FR-SVR-GWO models, the visual inspection of the ROC curves was considered for further
521 judgment about the performance of these models. The closer the ROC curves to the upper left
522 corner, the better the performance of the model can be seen (Tien Bui et al., 2016). As shown
523 in Figure 10b, the ROC curve of the FR-SVR-WOA model is closer to the upper left corner
524 compared to that of FR-SVR-GWO model implying on the better performance of that
525 compared to the FR-SVR-GWO model. According to the qualitative classification of AUC
526 values (Tien Bui et al., 2016), both the hybrid FR-SVR-WOA and FR-SVR-GWO models are
527 categorized as the models with very good efficiency (0.8-0.9).

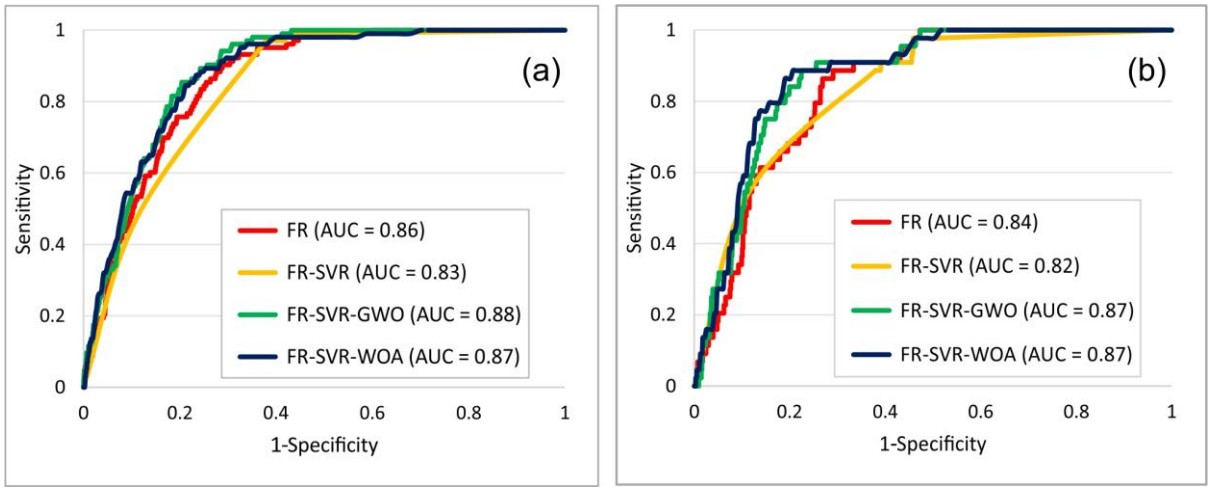

Figure 10. ROC curves of the developed hybrid models using a) train data b) test data

4.5. School flood risk map (SFRM)

The SFRM aids the authorities to direct the school vulnerability reduction plan to high-risk areas. The FRM was generated through the integration of school vulnerability indices (SVI) and FSM. As a result of the FR-SVR-WOA model superior performance and also the larger extent of the very high and high susceptibility classes on the WOA map; the FSM produced by this model (Figure 9c) was considered for FRM generation. Three SVI were considered for FRM generation namely: number of schools, number of students per each school, and the area of the school building. Figures 11a-b display the FRM in terms of the number of students and the area of the school building. On the maps, the size of circles is proportional to the number of students per each school and the area of the school building. By changing the color from blue to red, the probability of flooding is increased. As the SFRM show, southeastern parts of the Ardabil Province on the coastal areas are exposed to higher flood risk. Despite the small area of the buildings and less number of students per each school, the higher density of the schools in this region increases the potential flood damages. According to Table 3, 447 schools out of 1,208 schools (37%) and 44,362 students out of 130,773 students (33%) are exposed to the floods with high and very high probability of occurrence. It is worthy to note that the school area building is itself an indicator of the school resistance to flooding. The larger the area of the school building, the greater its flood

548 resistance. This increases the vulnerability to flooding and then increases the flood risk in this
549 region.

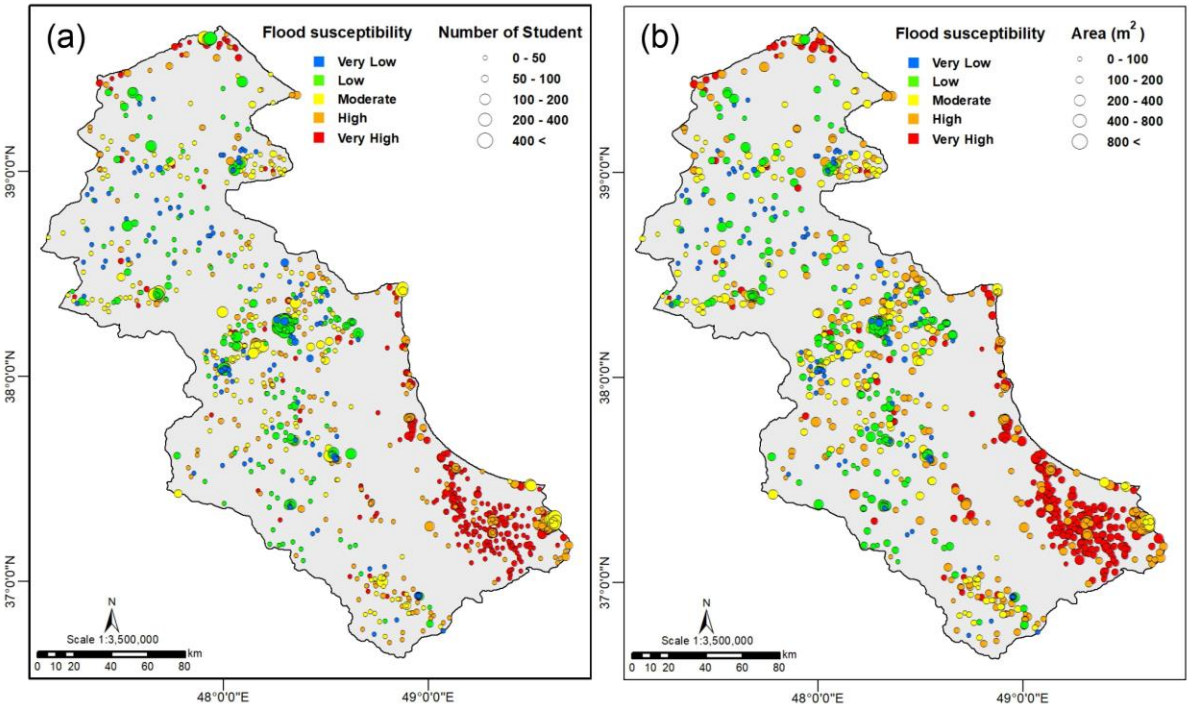

550
551 **Figure 11.** School Flood Risk Map (FRM): (a) number of students (b) school building area

552 **Table 3.** The number of schools and students exposed to flood risk

Susceptibility rate	Number of school	Number of student	area
Very low	195 (16.14%)	19836 (15.17%)	139925.5 (14.37%)
Low	312 (25.83%)	34067 (26.05%)	242192.5 (24.87%)
Moderate	254 (21.03%)	32508 (24.86%)	230550.5 (23.68%)
High	236 (19.54%)	27419 (20.97%)	214785.5 (22.06%)
Very high	211 (17.47%)	16943 (12.96%)	146227 (15.02%)

553 On the other hand, the schools located in southeastern and central parts of the Ardabil
554 Province are less vulnerable to flooding. They are also geographically close to the schools
555 with higher flood risks. The schools with less flooding risk and those survived during the

flooding can be served as crisis management centers in critical situations. The Red Crescent can use these schools as shelters to accommodate students, people, and injured people during the flooding. The results of this study provide prior awareness for the crisis management authorities to minimize the casualties by taking effective and timely decisions at the moment of the flooding. The crisis management authorities can minimize the loss lives by displacing the vulnerable people, children, and students to schools with less flooding risks.

5. Conclusions

The present study offered and assessed innovative intelligent-based meta-optimized hybrid models for risk mapping and flood susceptibility in a large-scale area to identifying the schools that are most vulnerable to flooding. The proposed methodology has not been investigated earlier and established here to take the advantages of meta-heuristic GWO and WOA algorithms for flood predictions in large scales. The proposed methodology was applied for Ardabil Province at western coastal areas of the Caspian Sea where the floods are a recurrent natural hazard. The results demonstrated that the FR-SVR-WOA and FR-SVR-GWO models yielded the best performance with AUC $\geq$ 0.87 which is a great achievement in an extent area under study. The FSM produced by WOA algorithm was used to generate the flood risk map as this algorithm classified larger parts of the area under study into very high susceptibility class. The results of this study demonstrated that the GWO algorithm has high processing speed which makes it suitable for large scale regions. One of the core findings of the present research is that WOA algorithm reproduced the higher FSI values comparing to GWO algorithm. This issue matters when dealing with the lives of humans especially with vulnerable communities such as young children. In these cases, the use of the WOA algorithm is preferred to the GWO algorithm. The FRM was constructed using the SVI and displayed the higher flood risks in southeastern coastal regions of the province where the schools are densely distributed. The results of this study recommend the authorities to direct

the flood mitigation strategies in the southeastern region of the province for reducing the school vulnerability to flooding by flood proofing the schools, establishing the flood alert systems and transferring and moving part of the students to safer sites. For modeling of flood susceptibility, the current research assumed the same flood conditioning factors for future flood events as to the past. However, the rainfall and land use factors have not the same influencing effects in the past and in the future owing to the climate and changes in land use. The future works are encouraged to consider the dynamic states of the climate and land use factors for flood susceptibility predictions.

Acknowledgments

This research was supported by the Basic Research Project of the Korea Institute of Geoscience and Mineral Resources (KIGAM) and Project of Environmental Business Big Data Platform and Center Construction funded by the Ministry of Science and ICT.

Compliance with ethical standards

Conflict of interest The authors declare that they have no confict of interest.

References

Ahmadlou, M., Al-Fugara, A., Al-Shabeeb, A.R., Arora, A., Al-Adamat, R., Pham, Q.B., Al-Ansari, N., Linh, N.T.T., Sajedi, H., 2021. Flood susceptibility mapping and assessment using a novel deep learning model combining multilayer perceptron and autoencoder neural networks. J. Flood Risk Manag. 14. https://doi.org/10.1111/jfr3.12683

Ahmadlou, M., Karimi, M., Alizadeh, S., Shirzadi, A., Parvinnejhad, D., Shahabi, H., Panahi, M., 2018. Flood susceptibility assessment using integration of adaptive network-based fuzzy inference system (ANFIS) and biogeography-based optimization (BBO) and BAT algorithms (BA). Geocarto Int. https://doi.org/10.1080/10106049.2018.1474276

Alade, I.O., Abd Rahman, M.A., Saleh, T.A., 2019. Modeling and prediction of the specific heat capacity of Al2O3/water nanofluids using hybrid genetic algorithm/support vector regression model. Nano-Structures and Nano-Objects. https://doi.org/10.1016/j.nanoso.2018.12.001

Ali, S.A., Parvin, F., Pham, Q.B., Vojtek, M., Vojteková, J., Costache, R., Linh, N.T.T., Nguyen, H.Q., Ahmad, A., Ghorbani, M.A., 2020. GIS-based comparative assessment of flood susceptibility mapping using hybrid multi-criteria decision-making approach, naïve Bayes tree, bivariate statistics and logistic regression: A case of Topľa basin, Slovakia. Ecol. Indic. 117, 106620. https://doi.org/10.1016/j.ecolind.2020.106620

Allafta, H., Opp, C., 2021. GIS-based multi-criteria analysis for flood prone areas mapping in the trans-boundary Shatt Al-Arab basin, Iraq-Iran. Geomatics, Nat. Hazards Risk 12, 2087–2116.

https://doi.org/10.1080/19475705.2021.1955755

Arabameri, A., Rezaie, F., Chandra Pal, S., Cerda, A., Saha, A., Chakrabortty, R., Lee, S., 2021a. Modelling of piping collapses and gully headcut landforms: Evaluating topographic variables from different types of DEM. Geosci. Front. 101230. https://doi.org/10.1016/j.gsf.2021.101230

Arabameri, A., Sadhasivam, N., Turabieh, H., Mafarja, M., Rezaie, F., Pal, S.C., Santosh, M., 2021b. Credal decision tree based novel ensemble models for spatial assessment of gully erosion and sustainable management. Sci. Rep. 11, 1–18. https://doi.org/10.1038/s41598-021-82527-3

Balogun, A.L., Rezaie, F., Pham, Q.B., Gigović, L., Drobnjak, S., Aina, Y.A., Panahi, M., Yekeen, S.T., Lee, S., 2021. Spatial prediction of landslide susceptibility in western Serbia using hybrid support vector regression (SVR) with GWO, BAT and COA algorithms. Geosci. Front. 12. https://doi.org/10.1016/j.gsf.2020.10.009

Band, S.S., Janizadeh, S., Chandra Pal, S., Saha, A., Chakrabortty, R., Melesse, A.M., Mosavi, A., 2020. Flash Flood Susceptibility Modeling Using New Approaches of Hybrid and Ensemble Tree-Based Machine Learning Algorithms. Remote Sens. 12, 3568. https://doi.org/10.3390/rs12213568

Breinl, K., Lun, D., Müller-Thomy, H., Blöschl, G., 2021. Understanding the relationship between rainfall and flood probabilities through combined intensity-duration-frequency analysis. J. Hydrol. 602, 126759. https://doi.org/10.1016/j.jhydrol.2021.126759

Bui, D.T., Khosravi, K., Li, S., Shahabi, H., Panahi, M., Singh, V.P., Chapi, K., Shirzadi, A., Panahi, S., Chen, W., Bin Ahmad, B., 2018a. New hybrids of ANFIS with several optimization algorithms for flood susceptibility modeling. Water (Switzerland). https://doi.org/10.3390/w10091210

Bui, D.T., Panahi, M., Shahabi, H., Singh, V.P., Shirzadi, A., Chapi, K., Khosravi, K., Chen, W., Panahi, S., Li, S., Ahmad, B. Bin, 2018b. Novel Hybrid Evolutionary Algorithms for Spatial Prediction of Floods. Sci. Rep. https://doi.org/10.1038/s41598-018-33755-7

Bui, D.T., Tsangaratos, P., Ngo, P.T.T., Pham, T.D., Pham, B.T., 2019. Flash flood susceptibility modeling using an optimized fuzzy rule based feature selection technique and tree based ensemble methods. Sci. Total Environ. https://doi.org/10.1016/j.scitotenv.2019.02.422

Cardenas, M.B., Wilson, J.L., Zlotnik, V.A., 2004. Impact of heterogeneity, bed forms, and stream curvature on subchannel hyporheic exchange. Water Resour. Res. https://doi.org/10.1029/2004WR003008

Centre for Research on the Epidemiology of Disasters, 201AD. Emergency Events Database [WWW Document]. Int. disasters database.

Cetisli, B., Edizkan, R., 2011. Estimation of adaptive neuro-fuzzy inference system parameters with the expectation maximization algorithm and extended Kalman smoother. Neural Comput. Appl. https://doi.org/10.1007/s00521-010-0406-4

Chen, W., Panahi, M., Khosravi, K., Pourghasemi, H.R., Rezaie, F., Parvinnezhad, D., 2019. Spatial prediction of groundwater potentiality using ANFIS ensembled with teaching-learning-based and biogeography-based optimization. J. Hydrol. 572, 435–448. https://doi.org/10.1016/j.jhydrol.2019.03.013

Chen, W., Panahi, M., Pourghasemi, H.R., 2017. Performance evaluation of GIS-based new ensemble data mining techniques of adaptive neuro-fuzzy inference system (ANFIS) with genetic algorithm (GA), differential evolution (DE), and particle swarm optimization (PSO) for landslide spatial modelling. Catena 157, 310–324. https://doi.org/10.1016/j.catena.2017.05.034

Choubin, B., Moradi, E., Golshan, M., Adamowski, J., Sajedi-Hosseini, F., Mosavi, A., 2019. An ensemble prediction of flood susceptibility using multivariate discriminant analysis, classification and regression trees, and support vector machines. Sci. Total Environ. 651, 2087–2096. https://doi.org/10.1016/j.scitotenv.2018.10.064

Costache, R., Arabameri, A., Elkhrachy, I., Ghorbanzadeh, O., Pham, Q.B., 2021. Detection of areas prone to flood risk using state-of-the-art machine learning models. Geomatics, Nat. Hazards Risk 12, 1488–1507. https://doi.org/10.1080/19475705.2021.1920480

Darabi, H., Haghighi, A.T., Mohamadi, M.A., Rashidpour, M., Ziegler, A.D., Hekmatzadeh, A.A., Kløve, B., 2020. Urban flood risk mapping using data-driven geospatial techniques for a flood-prone case area in Iran. Hydrol. Res. 51, 127–142. https://doi.org/10.2166/nh.2019.090

Das, S., Scaringi, G., 2021. River flooding in a changing climate: rainfall-discharge trends, controlling factors, and susceptibility mapping for the Mahi catchment, Western India. Nat. Hazards. https://doi.org/10.1007/s11069-021-04927-y

Dodangeh, E., Panahi, M., Rezaie, F., Lee, S., Tien Bui, D., Lee, C.W., Pradhan, B., 2020. Novel hybrid intelligence models for flood-susceptibility prediction: Meta optimization of the GMDH and SVR models with the genetic algorithm and harmony search. J. Hydrol. 590, 125423. https://doi.org/10.1016/j.jhydrol.2020.125423

Ewees, A.A., Elaziz, M.A., 2018. Improved Adaptive Neuro-Fuzzy Inference System Using Gray Wolf Optimization: A Case Study in Predicting Biochar Yield. J. Intell. Syst. 0. https://doi.org/10.1515/jisys-2017-0641

Faris, H., Aljarah, I., Al-Betar, M.A., Mirjalili, S., 2018. Grey wolf optimizer: a review of recent variants and applications. Neural Comput. Appl. 30, 413–435. https://doi.org/10.1007/s00521-017-3272-5

Fawcett, T., 2006. An introduction to ROC analysis. Pattern Recognit. Lett. 27, 861–874. https://doi.org/10.1016/j.patrec.2005.10.010

Fernández, D.S., Lutz, M.A., 2010. Urban flood hazard zoning in Tucumán Province, Argentina, using GIS and multicriteria decision analysis. Eng. Geol. https://doi.org/10.1016/j.enggeo.2009.12.006

Ghomian, Z., Yousefian, S., 2017. Natural Disasters in the Middle-East and North Africa With a Focus on Iran: 1900 to 2015. Heal. Emergencies Disasters Q. https://doi.org/10.18869/nrip.hdq.2.2.53

Ghosh, A., Kar, S.K., 2018. Application of analytical hierarchy process (AHP) for flood risk assessment: a case study in Malda district of West Bengal, India. Nat. Hazards 94, 349–368. https://doi.org/10.1007/s11069-018-3392-y

Gudiyangada Nachappa, T., Tavakkoli Piralilou, S., Gholamnia, K., Ghorbanzadeh, O., Rahmati, O., Blaschke, T., 2020. Flood susceptibility mapping with machine learning, multi-criteria decision analysis and ensemble using Dempster Shafer Theory. J. Hydrol. 590, 125275. https://doi.org/10.1016/j.jhydrol.2020.125275

Hamed, Y., Ibrahim Alzahrani, A., Shafie, A., Mustaffa, Z., Che Ismail, M., Kok Eng, K., 2020. Two steps hybrid calibration algorithm of support vector regression and K-nearest neighbors. Alexandria Eng. J. https://doi.org/10.1016/j.aej.2020.01.033

Hong, H., Panahi, M., Shirzadi, A., Ma, T., Liu, J., Zhu, A.X., Chen, W., Kougias, I., Kazakis, N., 2018. Flood susceptibility assessment in Hengfeng area coupling adaptive neuro-fuzzy inference system with genetic algorithm and differential evolution. Sci. Total Environ. https://doi.org/10.1016/j.scitotenv.2017.10.114

Huang, Y., Zhang, J., Tze Ann, F., Ma, G., 2020. Intelligent mixture design of steel fibre reinforced concrete using a support vector regression and firefly algorithm based multi-objective optimization model. Constr. Build. Mater. https://doi.org/10.1016/j.conbuildmat.2020.120457

İskenderoğlu, F.C., Baltacioğlu, M.K., Demir, M.H., Baldinelli, A., Barelli, L., Bidini, G., 2020. Comparison of support vector regression and random forest algorithms for estimating the SOFC output voltage by considering hydrogen flow rates. Int. J. Hydrogen Energy. https://doi.org/10.1016/j.ijhydene.2020.07.265

Jaafari, A., Panahi, M., Pham, B.T., Shahabi, H., Bui, D.T., Rezaie, F., Lee, S., 2019. Meta optimization of an adaptive neuro-fuzzy inference system with grey wolf optimizer and biogeography-based optimization algorithms for spatial prediction of landslide susceptibility. Catena 175, 430–445. https://doi.org/10.1016/j.catena.2018.12.033

Jenks, G., 1967. The data model concept in statistical mapping. Int. Yearb. Cartogr.

Kalantar, B., Ueda, N., Saeidi, V., Janizadeh, S., Shabani, Fariborz, Ahmadi, K., Shabani, Farzin, 2021. Deep Neural Network Utilizing Remote Sensing Datasets for Flood Hazard Susceptibility Mapping in Brisbane, Australia. Remote Sens. 13, 2638. https://doi.org/10.3390/rs13132638

Khoirunisa, N., Ku, C.-Y., Liu, C.-Y., 2021. A GIS-Based Artificial Neural Network Model for Flood Susceptibility Assessment. Int. J. Environ. Res. Public Health 18, 1072. https://doi.org/10.3390/ijerph18031072

Khosravi, K., Nohani, E., Maroufinia, E., Pourghasemi, H.R., 2016a. A GIS-based flood susceptibility

712 assessment and its mapping in Iran: a comparison between frequency ratio and weights-of-evidence bivariate
713 statistical models with multi-criteria decision-making technique. Nat. Hazards.
714 https://doi.org/10.1007/s11069-016-2357-2

715 Khosravi, K., Pham, B.T., Chapi, K., Shirzadi, A., Shahabi, H., Revhaug, I., Prakash, I., Tien Bui, D., 2018. A
716 comparative assessment of decision trees algorithms for flash flood susceptibility modeling at Haraz
717 watershed, northern Iran. Sci. Total Environ. https://doi.org/10.1016/j.scitotenv.2018.01.266

718 Khosravi, K., Pourghasemi, H.R., Chapi, K., Bahri, M., 2016b. Flash flood susceptibility analysis and its
719 mapping using different bivariate models in Iran: a comparison between Shannon's entropy, statistical index,
720 and weighting factor models. Environ. Monit. Assess. https://doi.org/10.1007/s10661-016-5665-9

721 Kumar, R., Acharya, P., 2016. Flood hazard and risk assessment of 2014 floods in Kashmir Valley: a space-
722 based multisensor approach. Nat. Hazards. https://doi.org/10.1007/s11069-016-2428-4

723 Lee, M.J., Kang, J.E., Jeon, S., 2012. Application of frequency ratio model and validation for predictive flooded
724 area susceptibility mapping using GIS. Int. Geosci. Remote Sens. Symp. 895–898.
725 https://doi.org/10.1109/IGARSS.2012.6351414

726 Leuenberger, M., Parente, J., Tonini, M., Pereira, M.G., Kanevski, M., 2018. Wildfire susceptibility mapping:
727 Deterministic vs. stochastic approaches. Environ. Model. Softw. 101, 194–203.
728 https://doi.org/10.1016/j.envsoft.2017.12.019

729 Los Huertos, M., 2020. Water Quality and Catchments, in: Ecology and Management of Inland Waters.
730 Elsevier, pp. 315–358. https://doi.org/10.1016/B978-0-12-814266-0.00024-6

731 McLay, C.D.A., Dragten, R., Sparling, G., Selvarajah, N., 2001. Predicting groundwater nitrate concentrations
732 in a region of mixed agricultural land use: A comparison of three approaches. Environ. Pollut.
733 https://doi.org/10.1016/S0269-7491(01)00111-7

734 McMaster, R., 1997. In Memoriam: George F. Jenks (1916-1996). Cartogr. Geogr. Inf. Syst. 24, 56–59.
735 https://doi.org/10.1559/152304097782438764

736 Mech, L.D., 1999. Alpha status, dominance, and division of labor in wolf packs. Can. J. Zool. 77, 1196–1203.
737 https://doi.org/10.1139/cjz-77-8-1196

738 Miles, R.E., Snow, C.C., 1984. Designing strategic human resources systems. Organ. Dyn.
739 https://doi.org/10.1016/0090-2616(84)90030-5

740 Mirjalili, S., Lewis, A., 2016. The Whale Optimization Algorithm. Adv. Eng. Softw. 95, 51–67.
741 https://doi.org/10.1016/j.advengsoft.2016.01.008

742 Mirjalili, S., Mirjalili, S.M., Lewis, A., 2014. Grey Wolf Optimizer. Adv. Eng. Softw. 69, 46–61.
743 https://doi.org/10.1016/j.advengsoft.2013.12.007

744 Mohammadi, B., Mehdizadeh, S., 2020. Modeling daily reference evapotranspiration via a novel approach
745 based on support vector regression coupled with whale optimization algorithm. Agric. Water Manag.
746 https://doi.org/10.1016/j.agwat.2020.106145

747 Mousavi, S.M., Roostaei, S., Rostamzadeh, H., 2019. Estimation of flood land use/land cover mapping by
748 regional modelling of flood hazard at sub-basin level case study: Marand basin. Geomatics, Nat. Hazards
749 Risk 10, 1155–1175. https://doi.org/10.1080/19475705.2018.1549112

750 Muro, C., Escobedo, R., Spector, L., Coppinger, R.P., 2011. Wolf-pack (Canis lupus) hunting strategies emerge
751 from simple rules in computational simulations. Behav. Processes 88, 192–197.
752 https://doi.org/10.1016/j.beproc.2011.09.006

753 Narimani, R., Jun, C., Shahzad, S., Oh, J., Park, K., 2021. Application of a Novel Hybrid Method for Flood
754 Susceptibility Mapping with Satellite Images: A Case Study of Seoul, Korea. Remote Sens. 13, 2786.
755 https://doi.org/10.3390/rs13142786

756 Nguyen, H.D., Nguyen, Q.-H., Du, Q.V.V., Nguyen, T.H.T., Nguyen, T.G., Bui, Q.-T., 2021. A novel
757 combination of deep neural network and Manta ray foraging optimization for flood susceptibility mapping in
758 Quang Ngai province, Vietnam. Geocarto Int. 1–25. https://doi.org/10.1080/10106049.2021.1975832

759 Norallahi, M., Seyed Kaboli, H., 2021. Urban flood hazard mapping using machine learning models: GARP,

RF, MaxEnt and NB. Nat. Hazards 106, 119–137. https://doi.org/10.1007/s11069-020-04453-3

Owolabi, T.O., 2019. Modeling the magnetocaloric effect of manganite using hybrid genetic and support vector regression algorithms. Phys. Lett. A 383, 1782–1790. https://doi.org/10.1016/j.physleta.2019.02.036

Panahi, M., Dodangeh, E., Rezaie, F., Khosravi, K., Van Le, H., Lee, M.J., Lee, S., Thai Pham, B., 2021. Flood spatial prediction modeling using a hybrid of meta-optimization and support vector regression modeling. Catena 199, 105114. https://doi.org/10.1016/j.catena.2020.105114

Panahi, M., Gayen, A., Pourghasemi, H.R., Rezaie, F., Lee, S., 2020. Spatial prediction of landslide susceptibility using hybrid support vector regression (SVR) and the adaptive neuro-fuzzy inference system (ANFIS) with various metaheuristic algorithms. Sci. Total Environ. 741, 139937. https://doi.org/10.1016/j.scitotenv.2020.139937

Park, S.-J., Lee, D.-K., 2020. Prediction of coastal flooding risk under climate change impacts in South Korea using machine learning algorithms. Environ. Res. Lett. 15, 094052. https://doi.org/10.1088/1748-9326/aba5b3

Pourghasemi, H.R., Kariminejad, N., Amiri, M., Edalat, M., Zarafshar, M., Blaschke, T., Cerda, A., 2020. Assessing and mapping multi-hazard risk susceptibility using a machine learning technique. Sci. Rep. 10, 3203. https://doi.org/10.1038/s41598-020-60191-3

Pradhan, B., 2010. Flood susceptible mapping and risk area delineation using logistic regression, GIS and remote sensing. J. Spat. Hydrol.

Predick, K.I., Turner, M.G., 2008. Landscape configuration and flood frequency influence invasive shrubs in floodplain forests of the Wisconsin River (USA). J. Ecol. https://doi.org/10.1111/j.1365-2745.2007.01329.x

Rahman, M., Ningsheng, C., Mahmud, G.I., Islam, M.M., Pourghasemi, H.R., Ahmad, H., Habumugisha, J.M., Washakh, R.M.A., Alam, M., Liu, E., Han, Z., Ni, H., Shufeng, T., Dewan, A., 2021. Flooding and its relationship with land cover change, population growth, and road density. Geosci. Front. 12, 101224. https://doi.org/10.1016/j.gsf.2021.101224

Rahmati, O., Pourghasemi, H.R., Zeinivand, H., 2016. Flood susceptibility mapping using frequency ratio and weights-of-evidence models in the Golastan Province, Iran. Geocarto Int. https://doi.org/10.1080/10106049.2015.1041559

Razavi Termeh, S.V., Kornejady, A., Pourghasemi, H.R., Keesstra, S., 2018. Flood susceptibility mapping using novel ensembles of adaptive neuro fuzzy inference system and metaheuristic algorithms. Sci. Total Environ. 615, 438–451. https://doi.org/10.1016/j.scitotenv.2017.09.262

Rufat, S., Tate, E., Burton, C.G., Maroof, A.S., 2015. Social vulnerability to floods: Review of case studies and implications for measurement. Int. J. Disaster Risk Reduct. https://doi.org/10.1016/j.ijdrr.2015.09.013

Samani, S., 2019. Allocation of 151 billion rials to compensate for flood damage to two provinces [WWW Document]. Iran. student's News Agency.

Schumann, G.J.-P., Vernieuwe, H., De Baets, B., Verhoest, N.E.C., 2014. ROC-based calibration of flood inundation models. Hydrol. Process. 28, 5495–5502. https://doi.org/10.1002/hyp.10019

Seejata, K., Yodying, A., Wongthadam, T., Mahavik, N., Tantanee, S., 2018. Assessment of flood hazard areas using Analytical Hierarchy Process over the Lower Yom Basin, Sukhothai Province. Procedia Eng. 212, 340–347. https://doi.org/10.1016/j.proeng.2018.01.044

Shafapour Tehrany, M., Kumar, L., Shabani, F., 2019. A novel GIS-based ensemble technique for flood susceptibility mapping using evidential belief function and support vector machine: Brisbane, Australia. PeerJ 7, e7653. https://doi.org/10.7717/peerj.7653

Shafapour Tehrany, M., Shabani, F., Neamah Jebur, M., Hong, H., Chen, W., Xie, X., 2017. GIS-based spatial prediction of flood prone areas using standalone frequency ratio, logistic regression, weight of evidence and their ensemble techniques. Geomatics, Nat. Hazards Risk 8, 1538–1561. https://doi.org/10.1080/19475705.2017.1362038

Shafizadeh-Moghadam, H., Valavi, R., Shahabi, H., Chapi, K., Shirzadi, A., 2018. Novel forecasting approaches using combination of machine learning and statistical models for flood susceptibility mapping. J. Environ.

Manage. https://doi.org/10.1016/j.jenvman.2018.03.089

Shahsavar, A., Bagherzadeh, S.A., Mahmoudi, B., Hajizadeh, A., Afrand, M., Nguyen, T.K., 2019. Robust Weighted Least Squares Support Vector Regression algorithm to estimate the nanofluid thermal properties of water/graphene Oxide–Silicon carbide mixture. Phys. A Stat. Mech. its Appl. 525, 1418–1428. https://doi.org/https://doi.org/10.1016/j.physa.2019.03.086

Sharma, V.K., Mishra, N., Shukla, A.K., Yadav, A., Rao, G.S., Bhanumurthy, V., 2017. Satellite data planning for flood mapping activities based on high rainfall events generated using TRMM, GEFS and disaster news. Ann. GIS 23, 131–140. https://doi.org/10.1080/19475683.2017.1304449

Shirzadi, A., Chapi, K., Shahabi, H., Solaimani, K., Kavian, A., Ahmad, B. Bin, 2017. Rock fall susceptibility assessment along a mountainous road: an evaluation of bivariate statistic, analytical hierarchy process and frequency ratio. Environ. Earth Sci. https://doi.org/10.1007/s12665-017-6471-6

Siam, Z.S., Hasan, R.T., Anik, S.S., Noor, F., Adnan, M.S.G., Rahman, R.M., 2021. Study of Hybridized Support Vector Regression Based Flood Susceptibility Mapping for Bangladesh. pp. 59–71. https://doi.org/10.1007/978-3-030-79463-7_6

Su, H., Li, X., Yang, B., Wen, Z., 2018. Wavelet support vector machine-based prediction model of dam deformation. Mech. Syst. Signal Process. 110, 412–427. https://doi.org/10.1016/j.ymssp.2018.03.022

Swain, K.C., Singha, C., Nayak, L., 2020. Flood Susceptibility Mapping through the GIS-AHP Technique Using the Cloud. ISPRS Int. J. Geo-Information 9, 720. https://doi.org/10.3390/ijgi9120720

Tavoosi, T., Delara, G., 2010. Climate Classification of Ardebil Province. Nivar 34, 47–52.

Tehrany, M.S., Pradhan, B., Jebur, M.N., 2015. Flood susceptibility analysis and its verification using a novel ensemble support vector machine and frequency ratio method. Stoch. Environ. Res. Risk Assess. https://doi.org/10.1007/s00477-015-1021-9

Tehrany, M.S., Pradhan, B., Jebur, M.N., 2014. Flood susceptibility mapping using a novel ensemble weights-of-evidence and support vector machine models in GIS. J. Hydrol. https://doi.org/10.1016/j.jhydrol.2014.03.008

Tehrany, M.S., Pradhan, B., Jebur, M.N., 2013. Spatial prediction of flood susceptible areas using rule based decision tree (DT) and a novel ensemble bivariate and multivariate statistical models in GIS. J. Hydrol. https://doi.org/10.1016/j.jhydrol.2013.09.034

Tien Bui, D., Pradhan, B., Nampak, H., Bui, Q.T., Tran, Q.A., Nguyen, Q.P., 2016. Hybrid artificial intelligence approach based on neural fuzzy inference model and metaheuristic optimization for flood susceptibilitgy modeling in a high-frequency tropical cyclone area using GIS. J. Hydrol. https://doi.org/10.1016/j.jhydrol.2016.06.027

Ullah, K., Zhang, J., 2020. GIS-based flood hazard mapping using relative frequency ratio method: A case study of panjkora river basin, eastern Hindu Kush, Pakistan. PLoS One 15, 1–18. https://doi.org/10.1371/journal.pone.0229153

UNISDR, 2015. Global Assessment Report on Disaster Risk Reduction., International Stratergy for Disaster Reduction (ISDR). https://doi.org/9789211320282

Vapnik, V.N., 1995. The Nature of Statistical Learning Theory, The Nature of Statistical Learning Theory. https://doi.org/10.1007/978-1-4757-2440-0

Wang, H., Xu, D., 2017. Parameter Selection Method for Support Vector Regression Based on Adaptive Fusion of the Mixed Kernel Function. J. Control Sci. Eng. https://doi.org/10.1155/2017/3614790

Waqas, H., Lu, L., Tariq, A., Li, Q., Baqa, M.F., Xing, J., Sajjad, A., 2021. Flash Flood Susceptibility Assessment and Zonation Using an Integrating Analytic Hierarchy Process and Frequency Ratio Model for the Chitral District, Khyber Pakhtunkhwa, Pakistan. Water 13, 1650. https://doi.org/10.3390/w13121650

Watkins, W.A., Schevill, W.E., 1979. Aerial Observation of Feeding Behavior in Four Baleen Whales: Eubalaena glacialis, Balaenoptera borealis, Megaptera novaeangliae, and Balaenoptera physalus. J. Mammal. 60, 155–163. https://doi.org/10.2307/1379766

Yalcin, A., Reis, S., Aydinoglu, A.C., Yomralioglu, T., 2011. A GIS-based comparative study of frequency

ratio, analytical hierarchy process, bivariate statistics and logistics regression methods for landslide susceptibility mapping in Trabzon, NE Turkey. Catena. https://doi.org/10.1016/j.catena.2011.01.014

Yao, W., Zhang, C., Hao, H., Wang, X., Li, X., 2018. A support vector machine approach to estimate global solar radiation with the influence of fog and haze. Renew. Energy. https://doi.org/10.1016/j.renene.2018.05.069

Yariyan, P., Avand, M., Abbaspour, R.A., Torabi Haghighi, A., Costache, R., Ghorbanzadeh, O., Janizadeh, S., Blaschke, T., 2020. Flood susceptibility mapping using an improved analytic network process with statistical models. Geomatics, Nat. Hazards Risk 11, 2282–2314. https://doi.org/10.1080/19475705.2020.1836036

Yates, D.N., Warner, T.T., Leavesley, G.H., 2002. Prediction of a Flash Flood in Complex Terrain. Part II: A Comparison of Flood Discharge Simulations Using Rainfall Input from Radar, a Dynamic Model, and an Automated Algorithmic System. J. Appl. Meteorol. https://doi.org/10.1175/1520-0450(2000)039<0815:poaffi>2.0.co;2

Yu, P.S., Chen, S.T., Chang, I.F., 2006. Support vector regression for real-time flood stage forecasting. J. Hydrol. https://doi.org/10.1016/j.jhydrol.2006.01.021

Yue, Z., Zhang, S., Xiao, W., 2020. A Novel Hybrid Algorithm Based on Grey Wolf Optimizer and Fireworks Algorithm. Sensors 20, 2147. https://doi.org/10.3390/s20072147

Yulianto, F., Suwarsono, Nugroho, U.C., Nugroho, N.P., Sunarmodo, W., Khomarudin, M.R., 2020. Spatial-Temporal Dynamics Land Use/Land Cover Change and Flood Hazard Mapping in the Upstream Citarum Watershed, West Java, Indonesia. Quaest. Geogr. 39, 125–146. https://doi.org/10.2478/quageo-2020-0010

Zzaman, R.U., Nowreen, S., Billah, M., Islam, A.S., 2021. Flood hazard mapping of Sangu River basin in Bangladesh using multi-criteria analysis of hydro-geomorphological factors. J. Flood Risk Manag. 14. https://doi.org/10.1111/jfr3.12715